Chapter 6
RELAY OPERATION DURING SECONDARY INJECTION TESTING

6.1 ABB REL531 Relay (Relay B)

Chapter 5 presented the reader with detailed system fault analysis for the relays under investigation. Problem areas that highlighted the need for relay setting changes were identified and corrections to relay settings were proposed. This chapter will focus on illustrating to the reader results that were obtained during secondary injection testing on protection relays whilst simulating different system conditions. These results highlights the impact that healthy phase and load currents for different system conditions could have on impedance relay reaches. It also aims to illustrate the vast difference in results that are obtained between the so-called "Classic" test method, which ignores healthy phase currents and tests which consider real system conditions.

6.1.1 Laboratory test results - classic method

This method uses a radial system with no load connected. The result is that for any fault on the feeder, the healthy phase currents are zero (i.e. the impact of charging and/or load current is ignored). The calculated positive and zero sequence line impedances that were used to determine the protection relay settings for the Bacchus – Droërivier line, were $Z_1 = 10.66 + j127.9\ \Omega$ and $Z_0 = 123.9 + j436.7\ \Omega$ respectively. The effective loop impedance is then $Z_{Loop} = 48.42 + j230.81\ \Omega$ primary. The zone 2 reach settings shown in the graphs to follow were set to 150% of line impedance to cater for the series capacitor on the line as per the manufacturers recommendation. The zone and phase selector settings as implemented were previously given in section 5.6.2. The resistive coverage for the zone phase-to-phase elements were set to 75 Ω/Loop, whilst that for the phase selector was set to 90.68 Ω/Loop. Fault resistances were simulated in primary ohms per loop (ie. the actual fault resistances were used in the simulations).

6.1.1.1 Single-phase-to-earth – measuring elements

In Figure 6.1 the theoretical characteristics of the REL531 relay's Zone and Phase Selector as originally implemented are shown, together with the tested reach values in the loop domain. It can be observed from the graph that the relay operates as per the theoretical calculated characteristics represented in the loop domain. Some deviation can be observed in the resistive reach.

The most important fact to note is that the Phase Selector element, which supervises the zone element, does not fully cover the resistive reach as set for the zone element. This will result in the maloperation of the zone element for faults, which it should be capable of detecting.

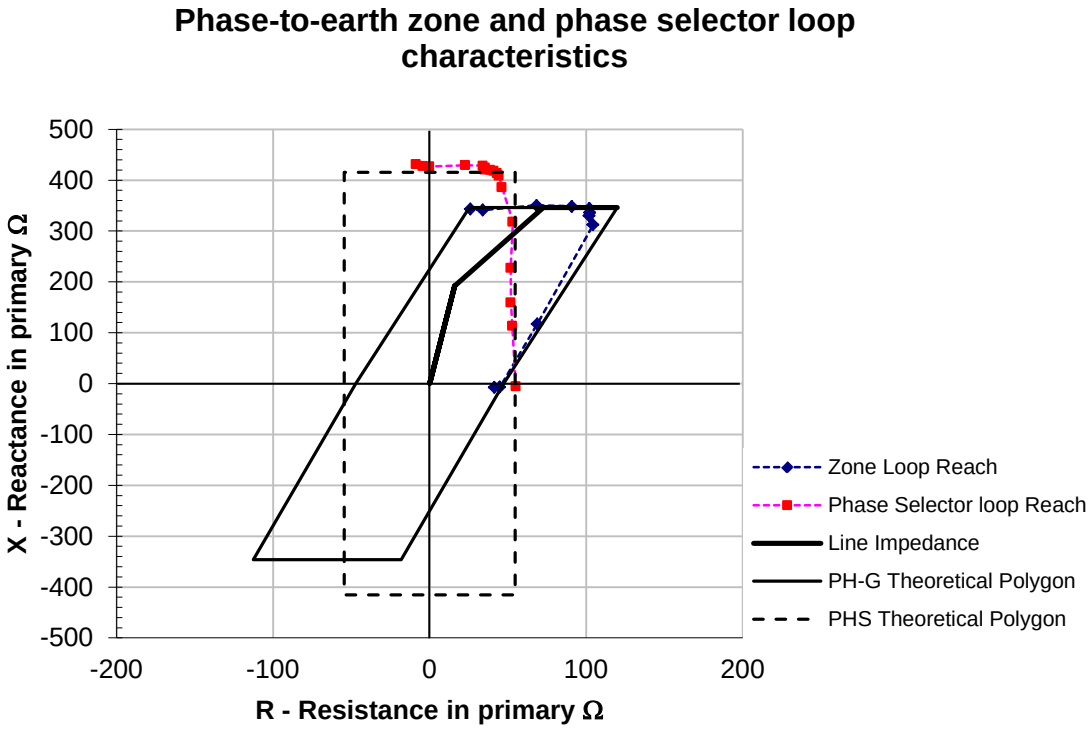

Figure 6.1: Phase-to-earth and phase selector characteristics with tested reach values

6.1.1.2 Phase-to-phase measuring elements

From Figure 6.2 it is evident that the relay operates as set for both the zone measuring element as well as the phase selector. Both characteristics have been plotted in the loop domain for simplicity and to be consistent with the plots shown for

the phase-to-earth faults. The calculations for the phase-to-phase zone elements, which are normally done in positive sequence, have been multiplied by a factor of 2 to be comparable with that of the phase selector. According to the graph it is possible that the relay may not operate for a phase-to-phase fault at the end of the line. To cater for this the phase selector's resistive reach would need to be increased.

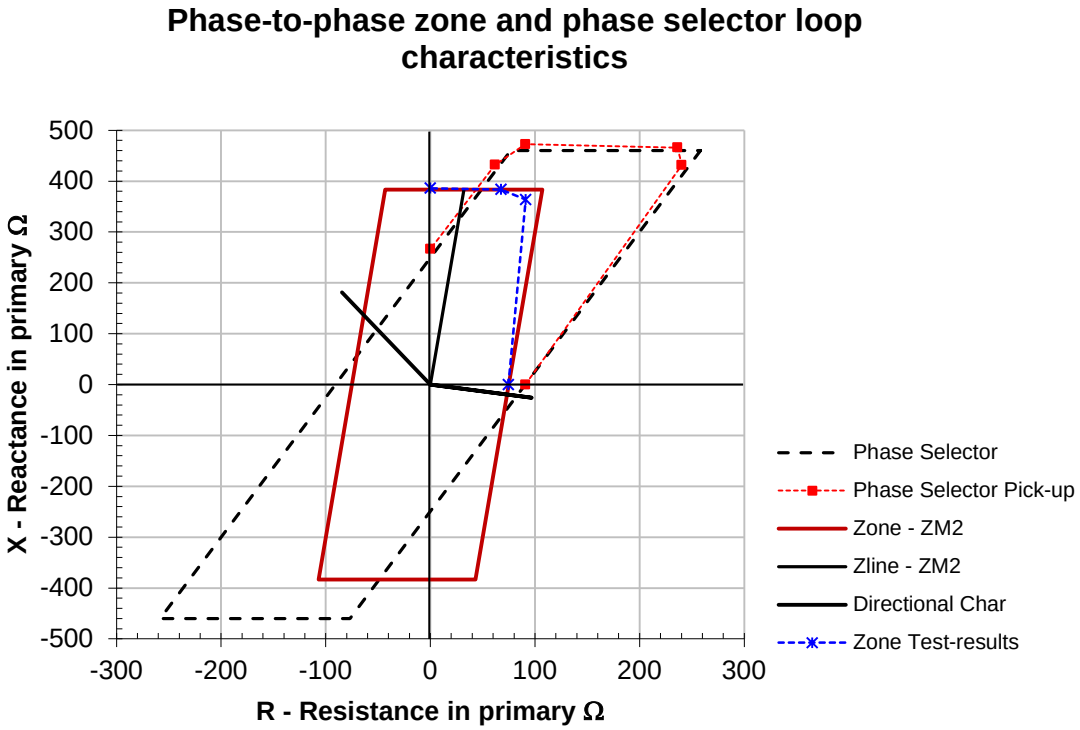

Figure 6.2: Phase-to-phase zone and phase selector characteristics with tested reach values

6.1.2 Impact of healthy phase currents on measurements

To illustrate the impact of the healthy phase current on the phase-to-earth and phase-to-phase measuring elements of this relay a few line faults with different fault resistive values at different locations on the line will be shown. It is essential to understand what this impact is, if any, in order to ensure optimal setting of the relay and therefore achieve the required performance on the network. System conditions such as remote end breaker open, power export and import were considered. The results of these tests are discussed in the sections below.

6.1.2.1 Radial feed with remote breaker open (capacitive charging)

6.1.2.1.1 Phase-to-earth faults at 50% of first line section

The PowerFactory system simulation software was used to simulate faults at different positions on this line with different fault resistances under varying system conditions. The results obtained with the remote end breaker open are discussed first. The impact of the charging current on the healthy phases are considered.

Figure 6.3 show the results obtained for a 25 Ω resistive fault at 50% of the first line section between Bacchus and Droërivier substations. Both the zone as well as the phase selector have measured the fault within its operating areas. It is important to note that both the zone and phase selector characteristics are shown in the loop domain. Figure 6.4 indicates the binary output signals recorded from the relay.

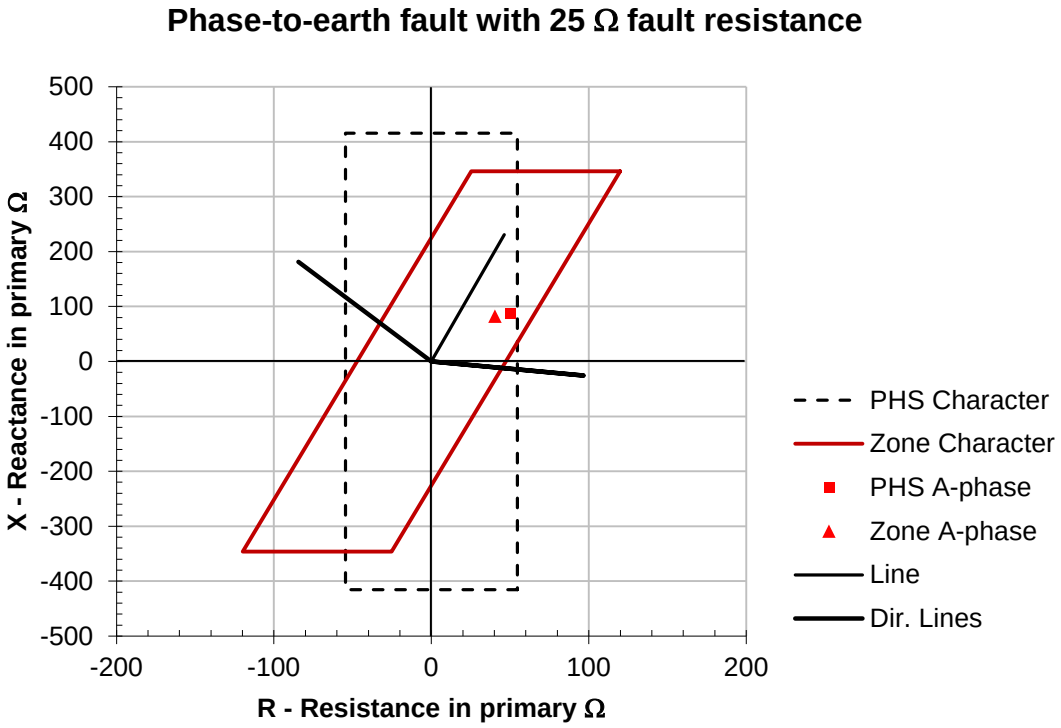

Figure 6.3: Phase-to-earth fault at 50% of first section of Bacchus-Droërivier line with 25 Ω resistive fault

Figure 6.4: Binary operating signals for phase-to-earth fault in Figure 6.3

The binary signals reflect the exact operation times of the different outputs recorded. Zone 4 (ZM4) was set with a trip time delay of 20 ms. All signals operated as expected. For a 40 Ω resistive fault at the same fault position only the zone measuring elements operated as can be seen when studying Figure 6.5 and Figure 6.6. Operation for the 40 Ω fault was only obtained from the current supervised zone 4 element. The phase selector measured the fault well outside its resistive reach and did not operate. Although this is a correct operation as per the applied setting, optimal operation of the relay was not achieved. As the phase selector supervises the zone 2 element, the zone 2 element could not operate due to a lack of resistive coverage of the phase selector. The resistive portion of the zone reach not covered by the phase selector can be observed from Figure 6.5. Operation of all instantaneous and permissive zones are supervised by the phase selector, in order to obtain phase selective tripping for this relay.

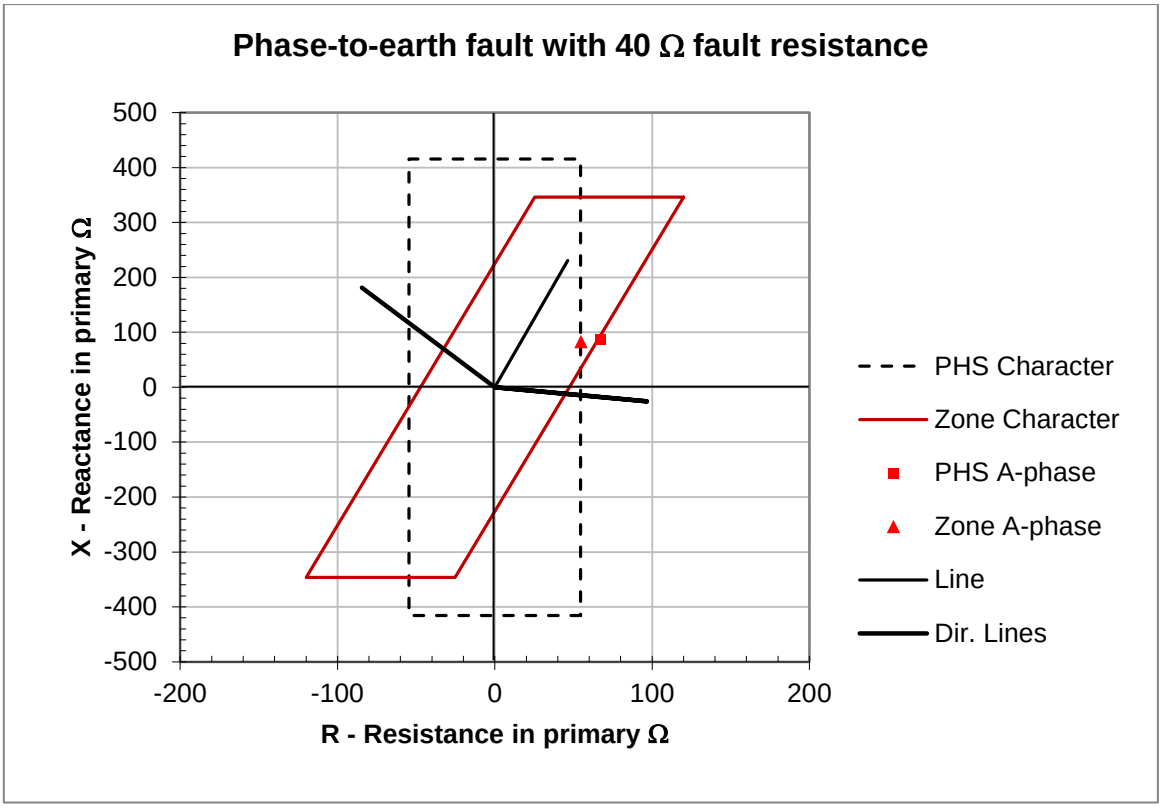

Figure 6.5: Phase-to-earth fault at 50% of first section of Bacchus-Droërivier line with 40 Ω resistive fault

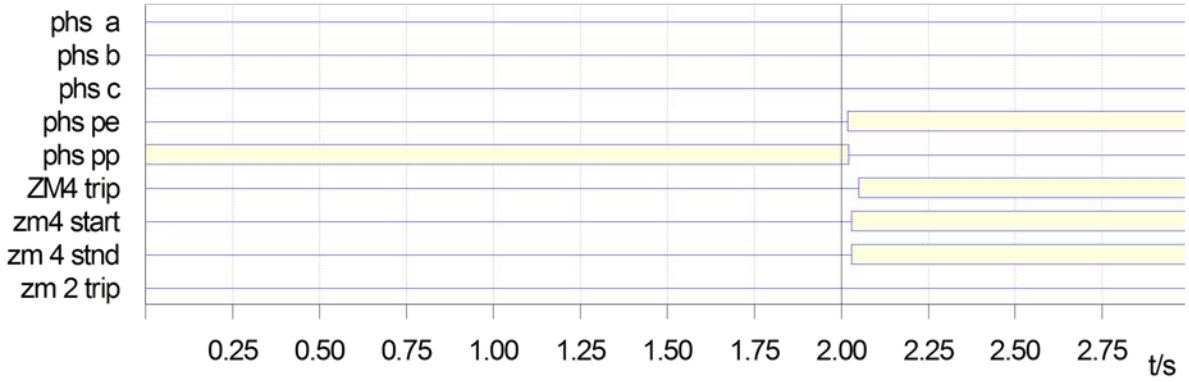

Figure 6.6: Binary operating signals for phase-to-earth fault in Figure 6.5

The results for a 45 Ω fault at 50% of the first line section of the Bacchus Droërivier line can be seen in Figure 6.7 and Figure 6.8. For this fault neither the phase selector nor the zone elements for both zone 2 and zone 4 operated. The zone element measurement in this case is a border line situation, whilst that for the phase selector is a clear non-operation scenario.

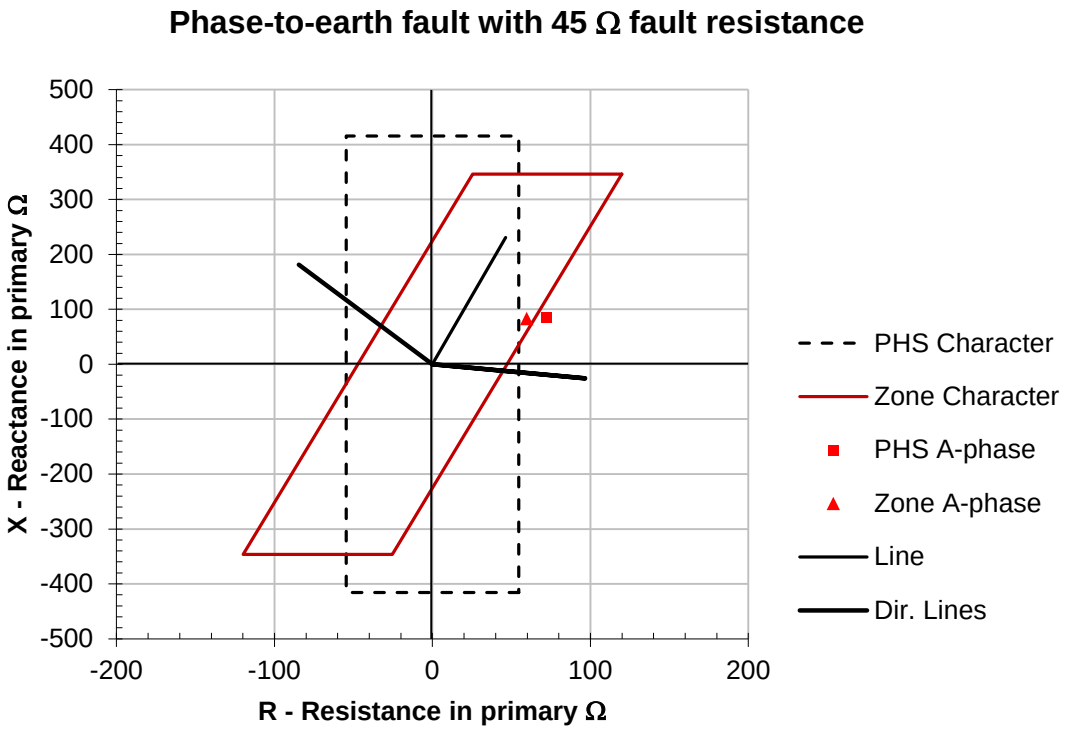

Figure 6.7: Phase-to-earth fault at 50% of first section of Bacchus-Droërivier line with 45 Ω resistive fault

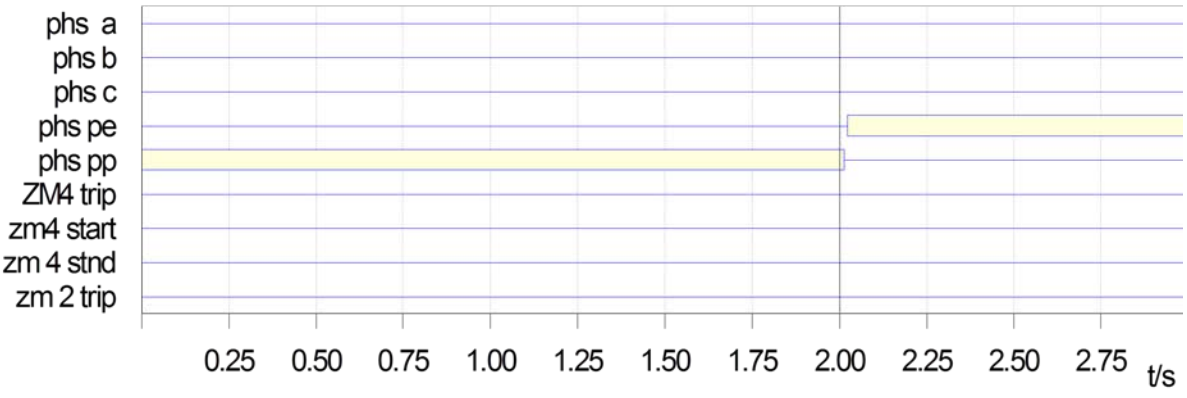

Figure 6.8: Binary operating signals for phase-to-earth fault in Figure 6.7

6.1.2.1.2 Phase-to-earth faults at end of line

For a bolted fault at the end of the Bacchus-Droërivier line, the Phase Selector does not detect the fault, and therefore the zone 2 element also does not operate, even though the measured impedance is within its reach. The current supervised zone 4 operates as can be seen from the binary signals of Figure 6.10.

The next fault simulated had a fault rsistance of 35 Ω. Only the current supervised zone 4 element operated for this fault as demonstated in Figure 6.11 and Figure 6.12. Although the impedance measurement is shown to be well within the zone reach, the binary signals clearly show a delayed and intermittent pick-up of the element. Comparing these results with the theoretical characteristic plots and test results shown in section 6.1 highlights the impact on the faulted phase of the capacitive charging current in the healthy phases. The capacitive charging current in the healthy phases therefore results in an underreaching of the zone measuring element. The relay's zone 2 element, although within its set reach, did not operate as expected since the phase selector measured the impedance well outside its set reach in the resistive direction (see Figure 6.11 and Figure 6.12).

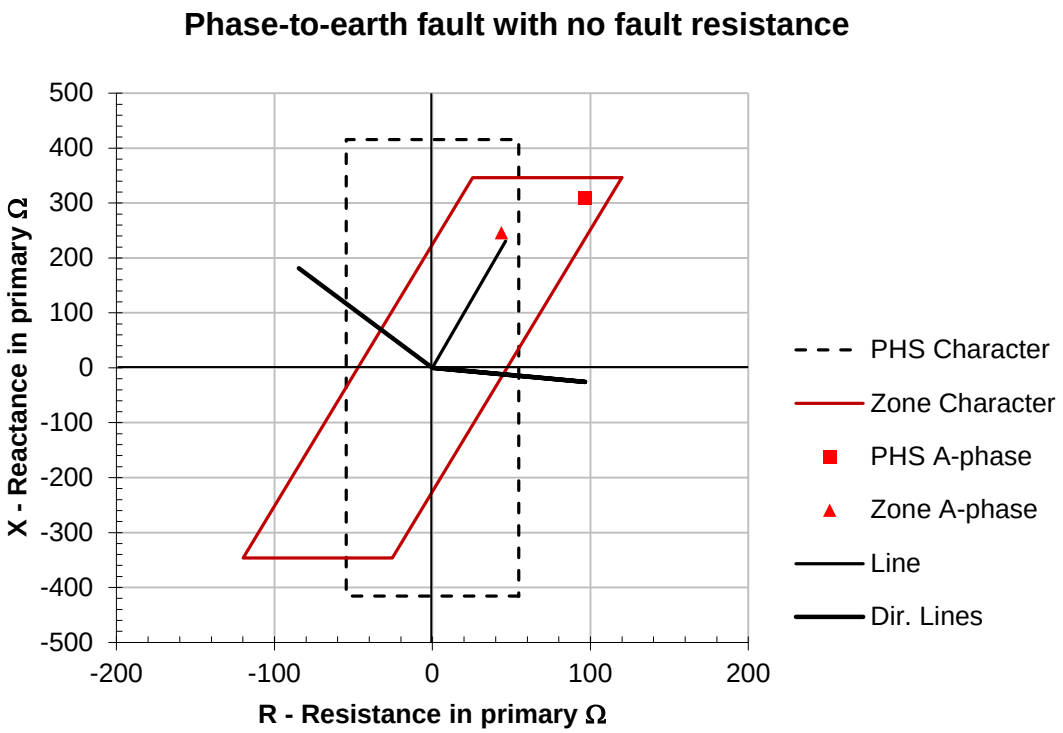

Figure 6.9: Phase-to-earth fault at the end of Bacchus-Droërivier line with no fault resistance

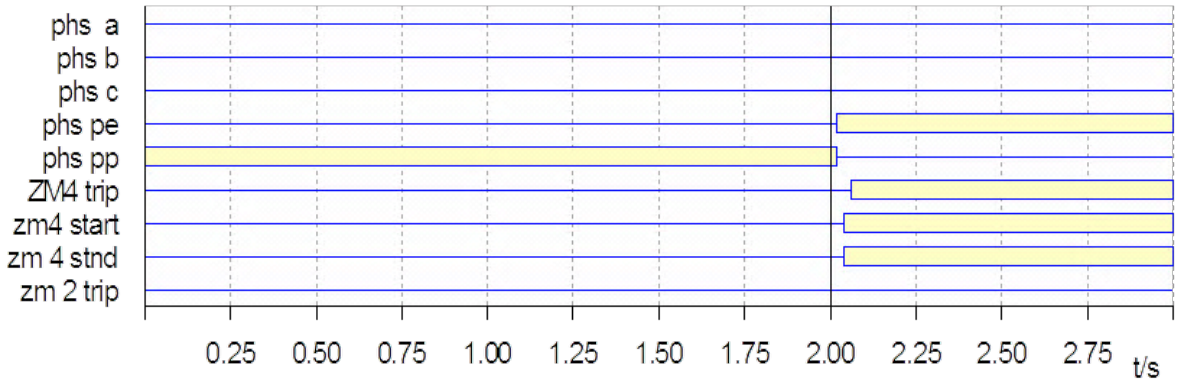

Figure 6.10: Binary operating signals for phase-to-earth fault in Figure 6.9

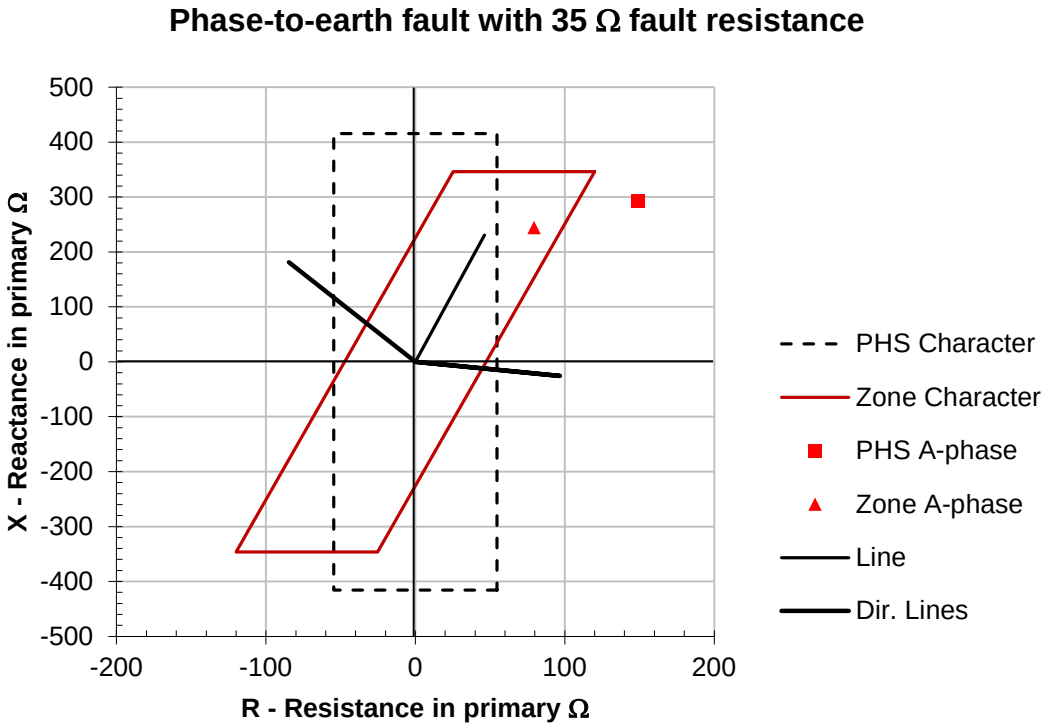

Figure 6.11: Phase-to-earth fault at the end of Bacchus-Droërivier line with 35 Ω fault resistance

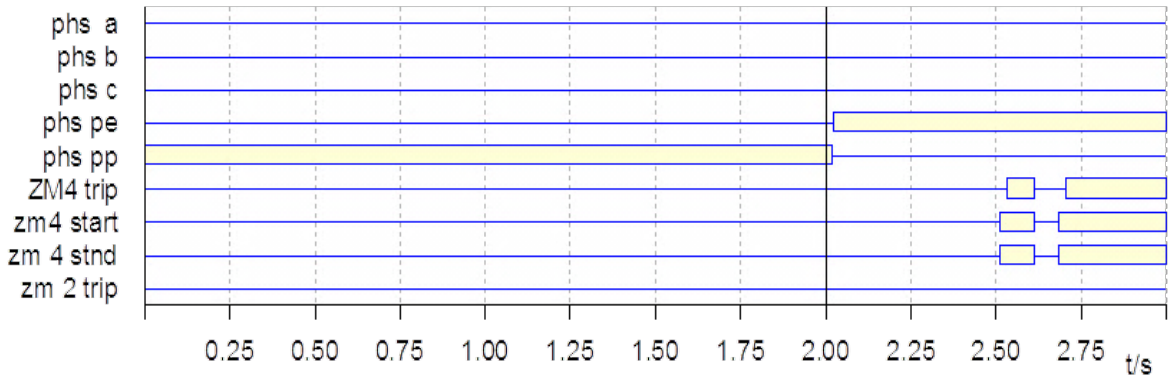

Figure 6.12: Binary operating signals for phase-to-earth fault in Figure 6.11

For a 40 Ω fault at the end of the line no operation of any zone measuring element or for the phase selector occurs (see Figure 6.13 and Figure 6.14). The zone impedance measurement indicates that the zone element should have picked up for this fault, whilst the phase selector measurement indicates no operation of this element. This phenomenon can be explained in part using the equation for positive sequence zone measurement;

$$Z_a = \frac{V_a}{(I_a + 3I_o K_o)} \qquad (6.1)$$

With the remote end breaker open, the value of the earth return current ($3I_o$) is equal to the phase current (I_a) (classic method), when the capacitive charging currents in the healthy phases are ignored. This is however, not the case in a real system, and therefore $3I_o$ is not equal to I_a. When the result of the sum of $I_a + 3I_0$ is smaller than $2I_a$, the value of the measured impedance increases, thus resulting in underreaching. The converse is true when $I_a + 3I_0$ is bigger than $2I_a$, which will result in overreaching. When comparing the maximum resistive reach results obtained in Figure 6.12 with that obtained with no currents in the healthy phases as shown in Figure 6.1, the following is apparent

From Figure 6.1 (No current in healthy phases):-

R_f measured is approximately 45 Ω

From Figure 6.13 (Charging current in Healthy phases):-

R_f measured is approximately 36.45 Ω

The deviation in the resistive fault measurements obtained, between the no current and charging current in healthy phases, implies that the capacitive charging currents in the healthy phases cause the zone measuring elements to only achieve pickup at smaller fault resistance values for a fault at the same location. The relay underreaches since it is not capable of detecting the same fault resistance as was possible without charging current.

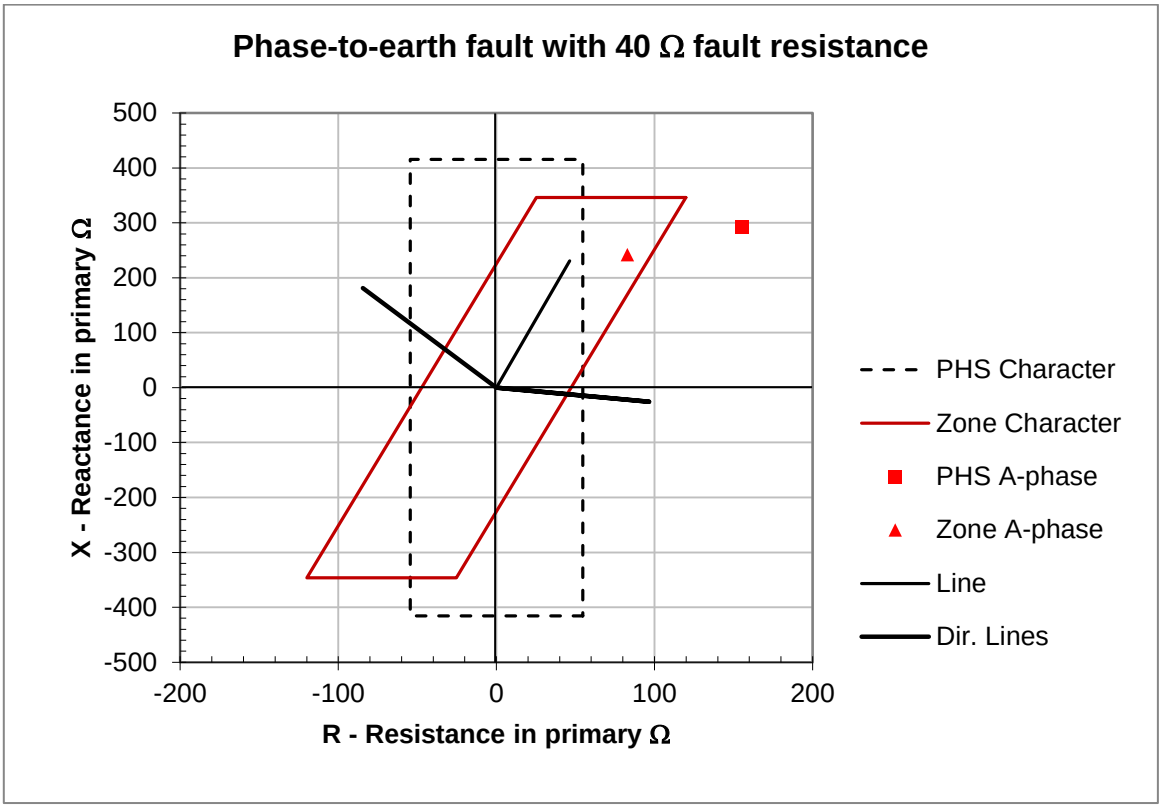

Figure 6.13: Phase-to-earth fault at the end of Bacchus-Droërivier line with 40 Ω fault resistance

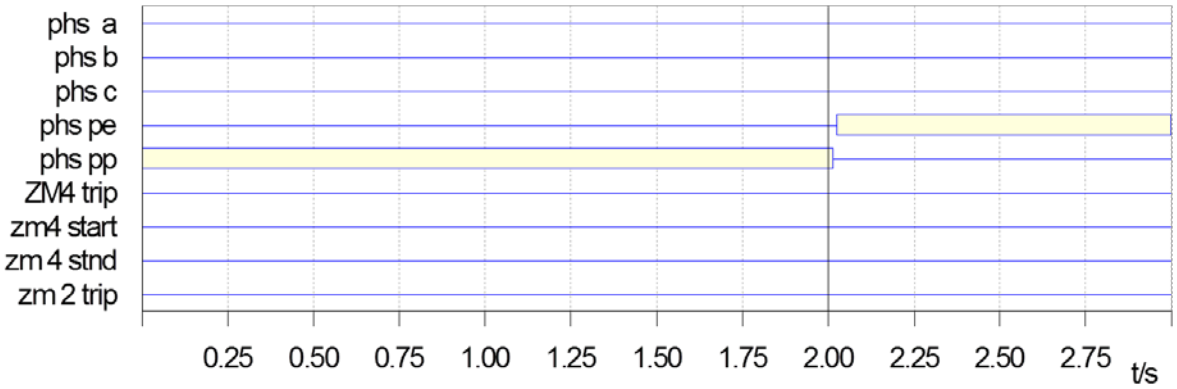

Figure 6.14: Binary operating signals for Phase-to-Earth fault in Figure 6.13

6.1.2.1.3 Phase-to-phase faults at series capacitor

The effect of the capacitive charging current of the healthy phase on the faulted phases seems to rotate the relay's characteristic anti-clockwise. The impact of this phenomenon is less for a bolted fault than for a 55 Ω fault at the same fault position, as can been seen when comparing Figure 6.2 to Figure 6.15. Figure 6.2 shows the maximum resistive pick-up with the remote end breaker open and no charging current on the healthy phase, whilst Figure 6.15 shows the maximum resistive pick-up under the same system condition, but with charging current on the healthy phase. This result shows that the effect of charging current and the capacitive coupling between phases cannot be ignored. The binary signals shown in Figure 6.16 and Figure 6.17 indicate that both the zone and phase selector measuring elements picked-up for the bolted and 55 Ω resistive faults. For a 60 Ω fault, the results of which are shown in Figure 6.18 and Figure 6.19, only the phase selector picked up. Considering the set phase-to-phase resistive reach of 75 Ω again shows a tendency to underreach under charging current conditions.

Phase-to-phase fault with a bolted and 55 Ω fault resistance

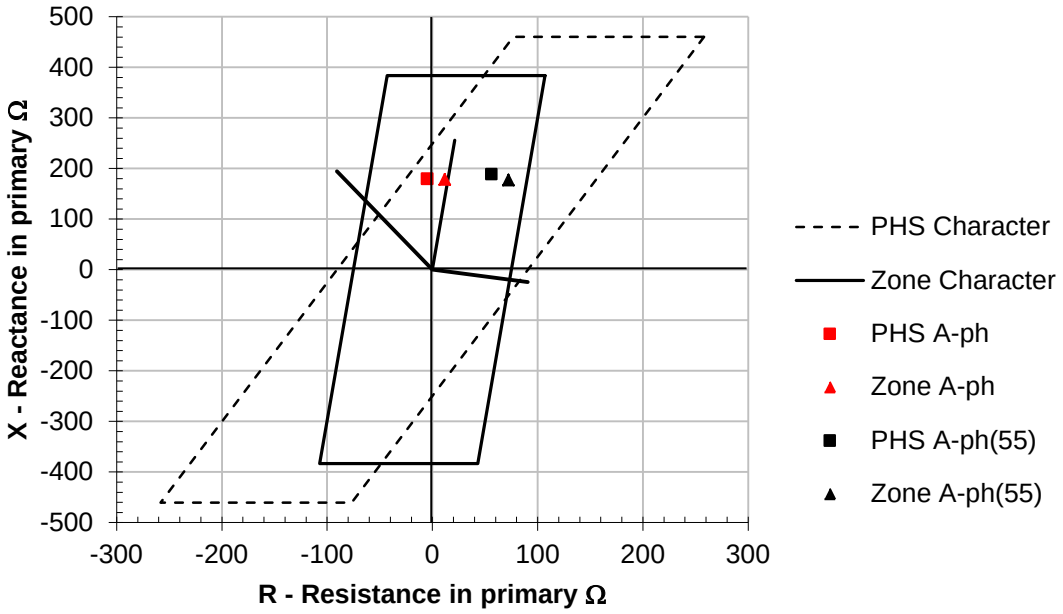

Figure 6.15: Phase-to-phase faults at Droërivier end of series capacitor with remote end breaker open (a bolted and 55 Ω fault is shown respectively)

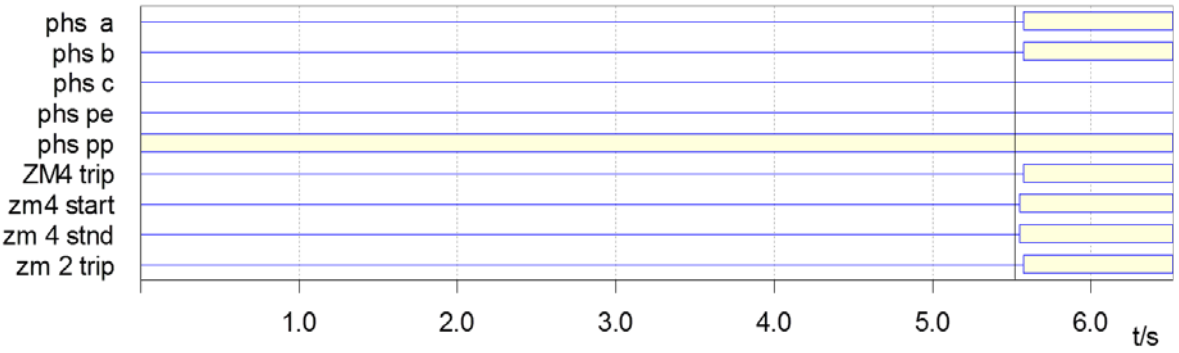

Figure 6.16: Binary signals for bolted fault at Droërivier end of series capacitor

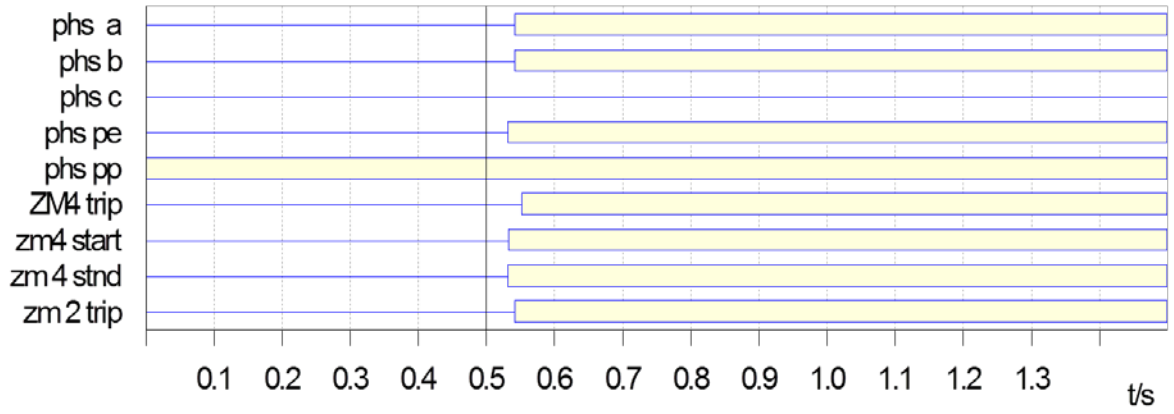

Figure 6.17: Binary signals for 55 Ω fault at Droërivier end of series capacitor

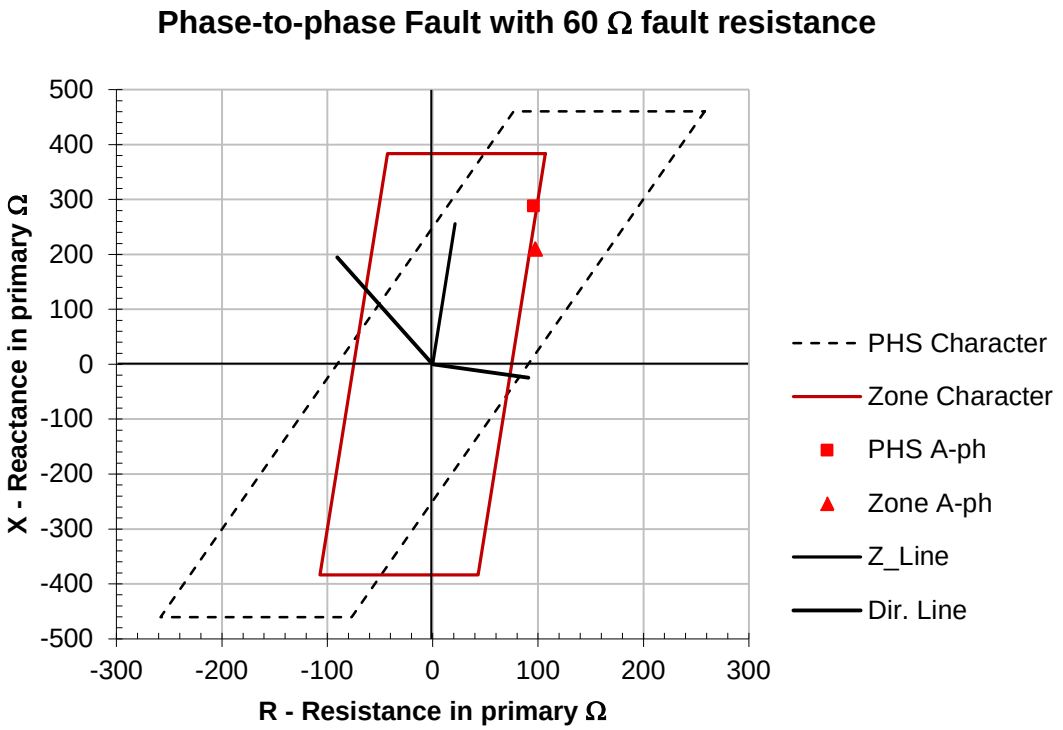

Figure 6.18: Phase-to-phase faults at Droërivier end of series capacitor with remote end breaker open (a 60 Ω fault is shown)

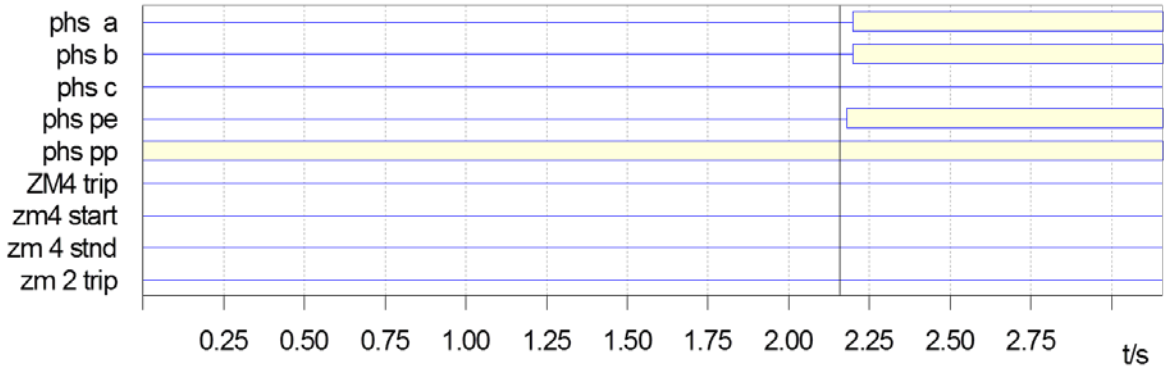

Figure 6.19: Binary signals for 60 Ω fault at Droërivier end of series capacitor (see figure 77)

6.1.2.1.4 Phase-to-phase faults at end of line

The fault position indicated by the zone reach measurement in Figure 6.20 is for a fault at the end of the Bacchus-Droërivier line. Pickup for the zone 4 element (current supervised), which was set the same as for the zone 2 element was achieved, but not for the phase selector. The binary signals for this event shown in

Figure 6.21 confirms this statement. With the remote end breaker in the open position, the phase selector therefore seriously underreaches.

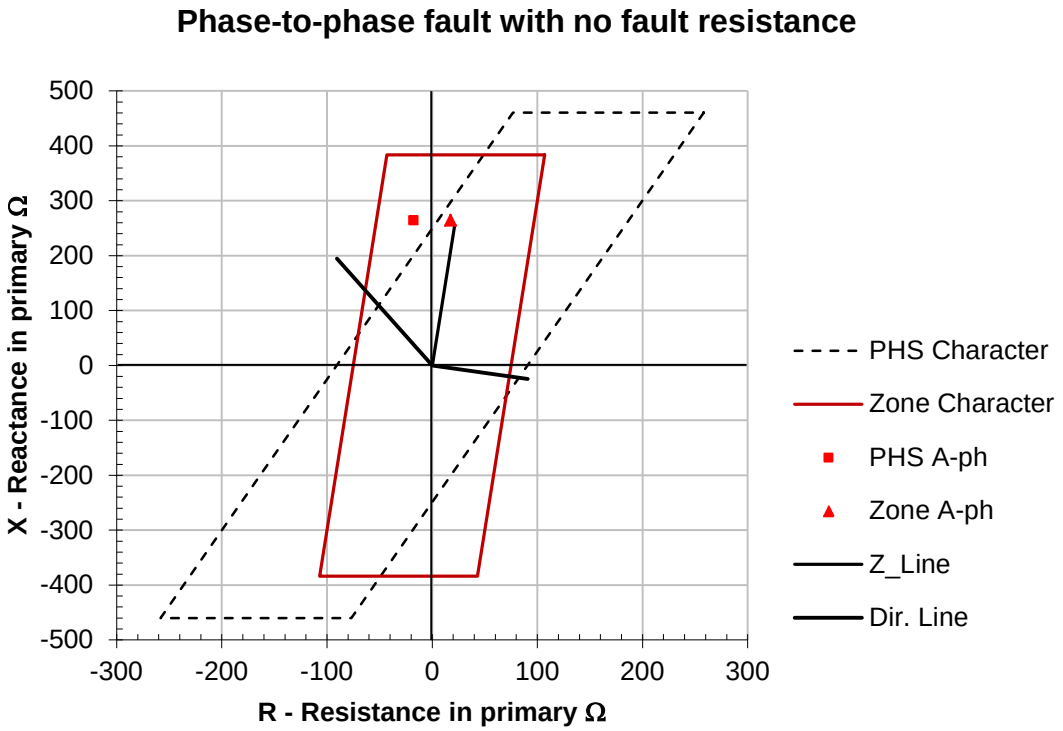

Figure 6.20: Phase-to-phase faults at end of line with remote end breaker open (a bolted fault is shown)

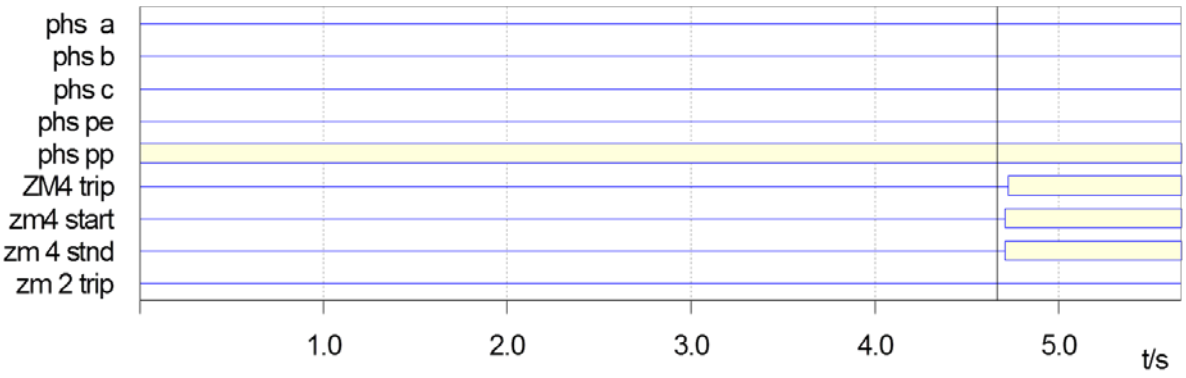

Figure 6.21: Binary signals for fault at end of line (see Figure 6.20)

6.1.3 Load current and remote in-feed

6.1.3.1 Exporting MW and Mvar – remote breaker closed

The next step was aimed at determining whether the zone measuring elements would be influenced by load current and remote end in-feed. Simulations were performed during load export conditions of approximately 1000 MW and 580 Mvar.

6.1.3.1.1 Phase-to-earth measurement

Pick-up of the zone element for a 47.5 Ω fault at 50% of the first section of the Bacchus-Droërivier line was obtained as shown in Figure 6.22 and Figure 6.23. This operation was obtained for a fault just outside the theoretical zone resistive reach. With the phase-to-earth fault resistance set to 47.3 Ω/Loop primary no obvious conclusions can be reached with regards to the impact of load current or remote end infeed for this fault. No operation was obtained for a 50 Ω fault and is not shown.

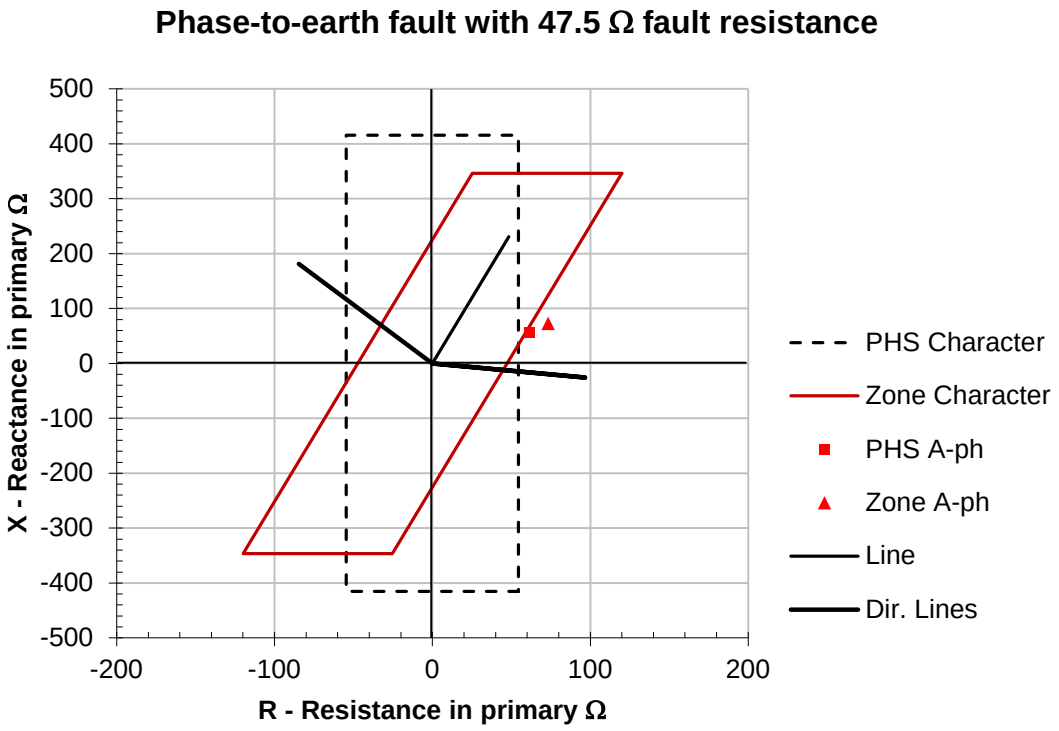

Figure 6.22: Phase-to-earth fault at 50% of the first section of Bacchus-Droërivier line with 47.5 Ω fault resistance (exporting load)

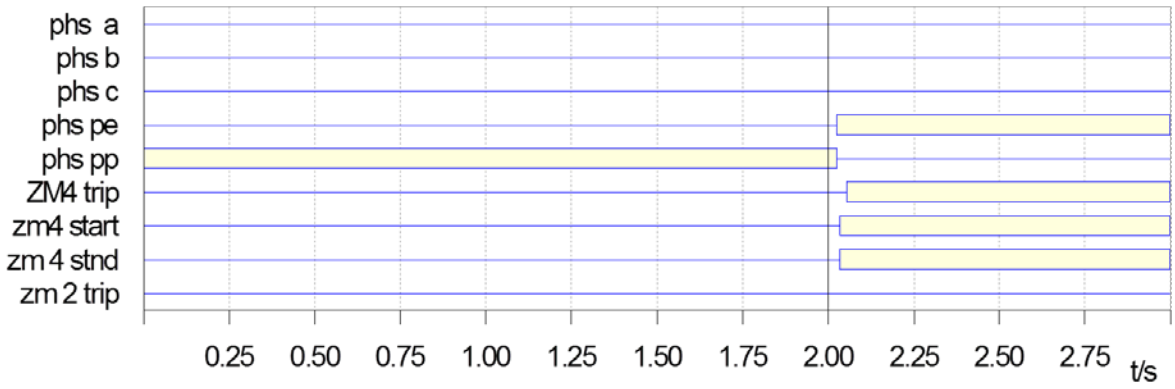

Figure 6.23: Binary operating signals for phase-to-earth fault in Figure 6.22

The next step was to determine any impact over the total length of the line. Operation of the zone measuring elements was only obtained for a 5 Ω resistive fault at this position. The measured resistance by the zone element for this fault was calculated to be 111.67 Ω per loop primary. Complete calculations are shown in an Excel file located in Appendix H. From Figure 6.24 it can be seen that the measured reach should have been outside the resistive reach coverage as theoretically defined. Two observations can be made (1) the effective fault resistance as determined by the relay has been enlarged significantly by the remote end in-feed into the fault, and (2) the export load current contributed to the relay's ability to detect this fault.

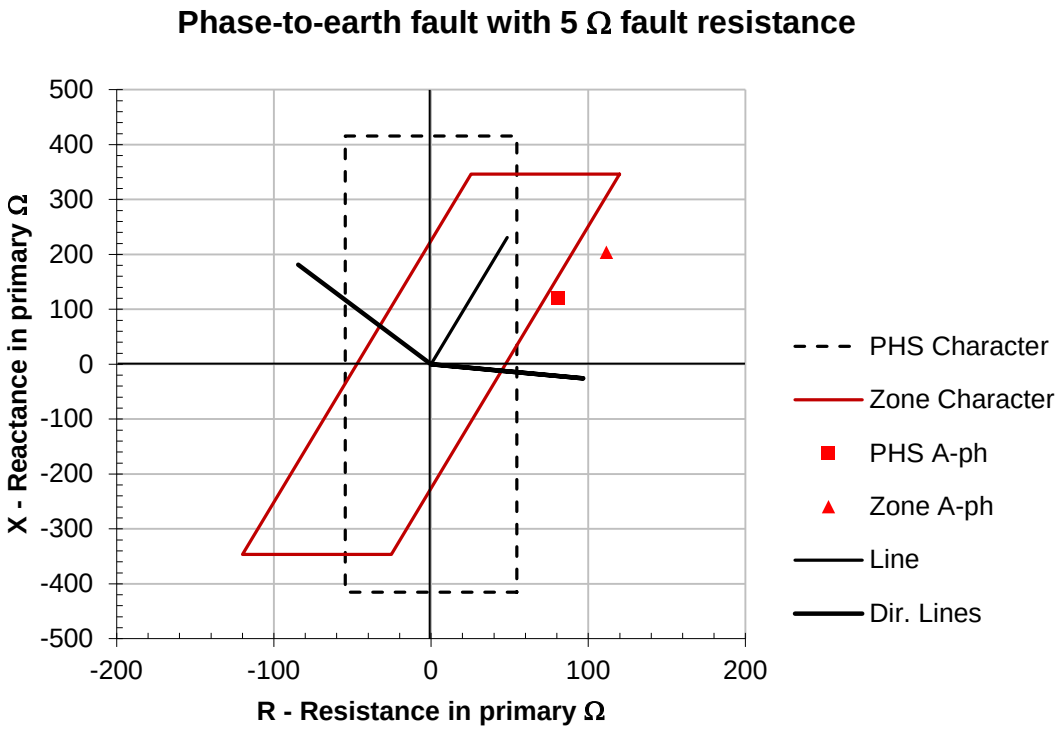

Figure 6.24: Phase-to-earth fault at the end of Bacchus-Droërivier line with 5 Ω fault resistance (exporting load)

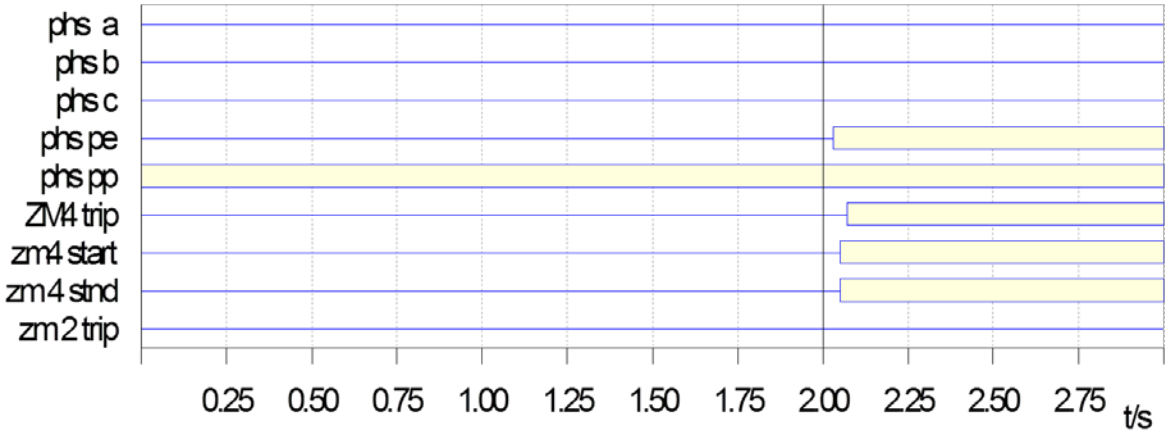

Figure 6.25: Binary operating signals for phase-to-earth fault in Figure 6.24

6.1.3.1.2 Phase-to-phase measurement

For a 65 Ω fault at 50% of the first section of the Bacchus-Droërivier line, both the zone and phase selector elements operated as expected. (see Figure 6.26 and Figure 6.27.) The zone reach is shown to be at a maximum. For a simulated 70 Ω resistive fault at the same location, the results of which are shown in Figure 6.28 and

Figure 6.29 only the phase selector pick-up was realised. Considering the fault resistive setting of 75 Ω for this element the relay therefore underreaches.

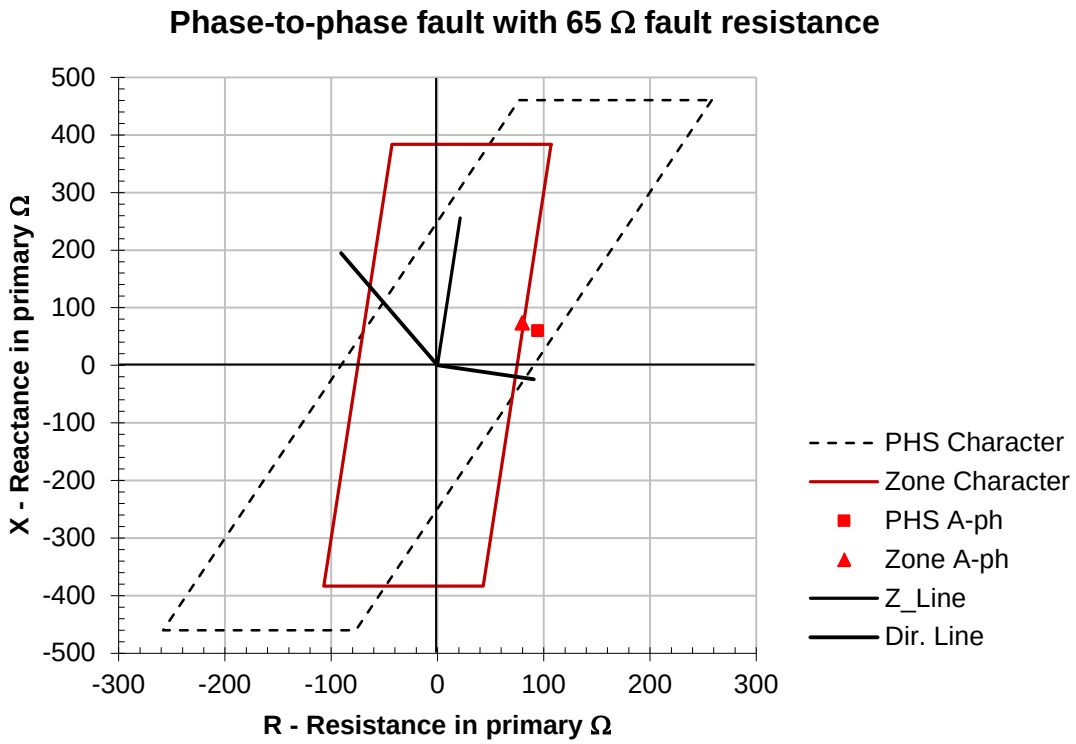

Figure 6.26: Phase-to-phase faults at 50% of first line section with exporting MW and Mvar (a 65 Ω fault is shown)

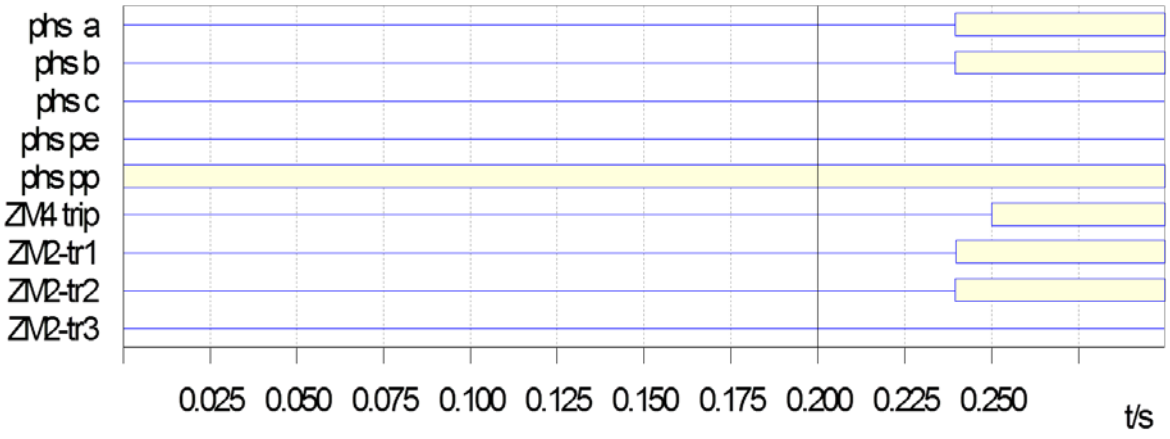

Figure 6.27: Binary signals for fault at 50% of first section of line

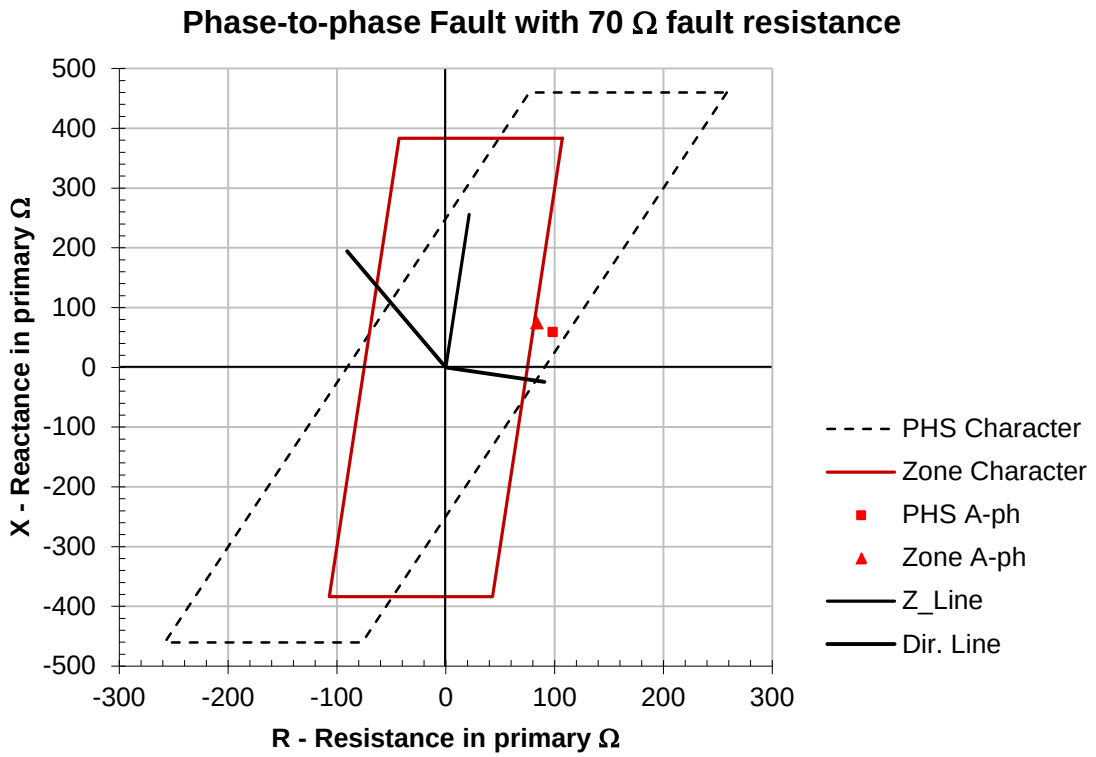

Figure 6.28: Phase-to-phase faults at 50% of first line section with exporting MW and Mvar (a 70 Ω fault is shown)

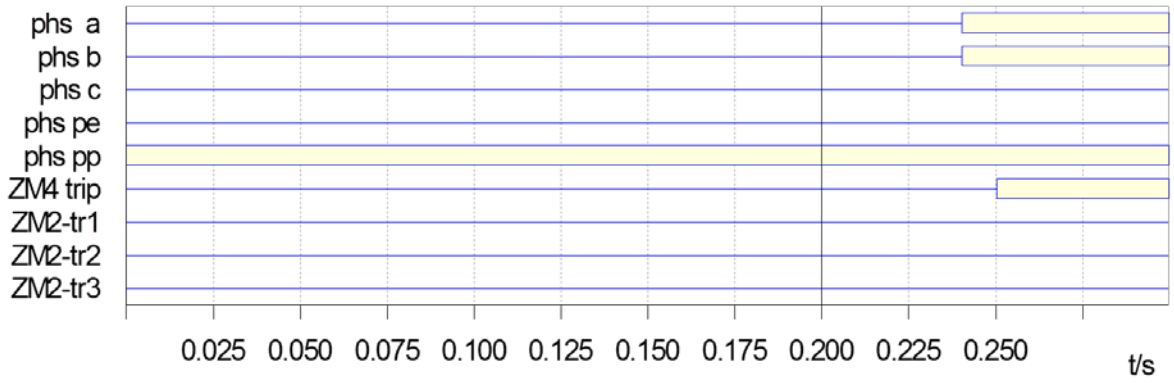

Figure 6.29: Binary signals for fault at 50% of first section of line

6.1.3.2 Importing MW and Mvar – remote breaker closed

6.1.3.2.1 Phase-to-earth measurement

A simulation was done with an approximate importing load of 1000 MW and 564 Mvar. Reach results was obtained for faults at 50% of the first line section.

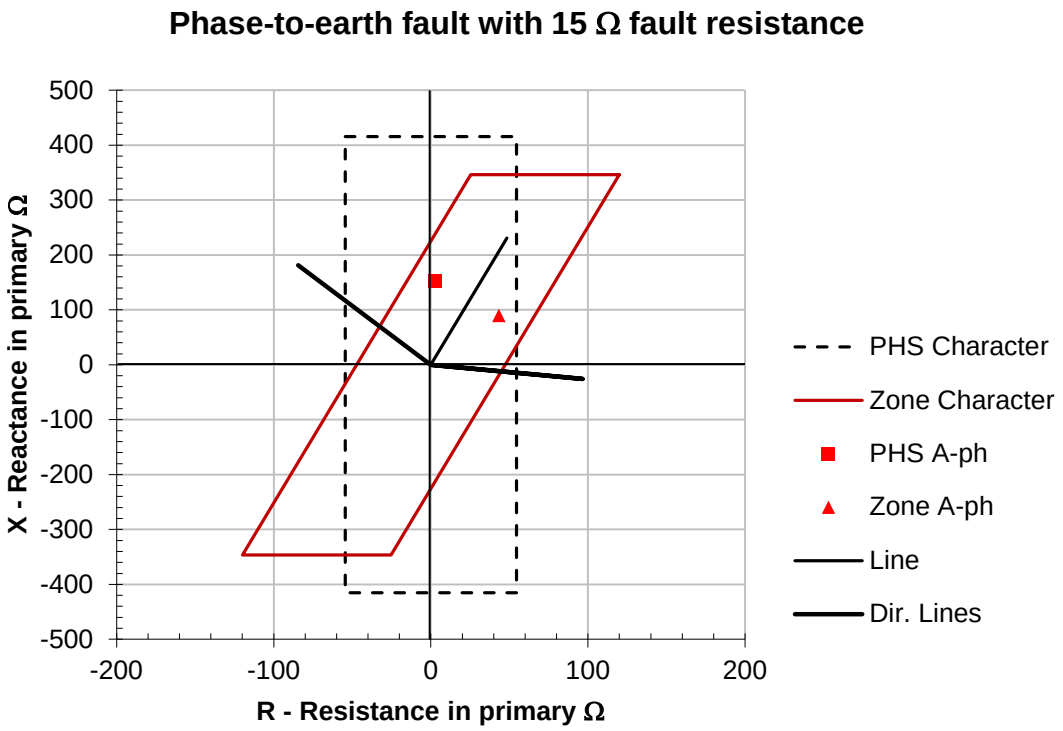

Figure 6.30: Phase-to-earth fault at 50% of the first section of Bacchus-Droërivier line with 15 Ω fault resistance (importing load)

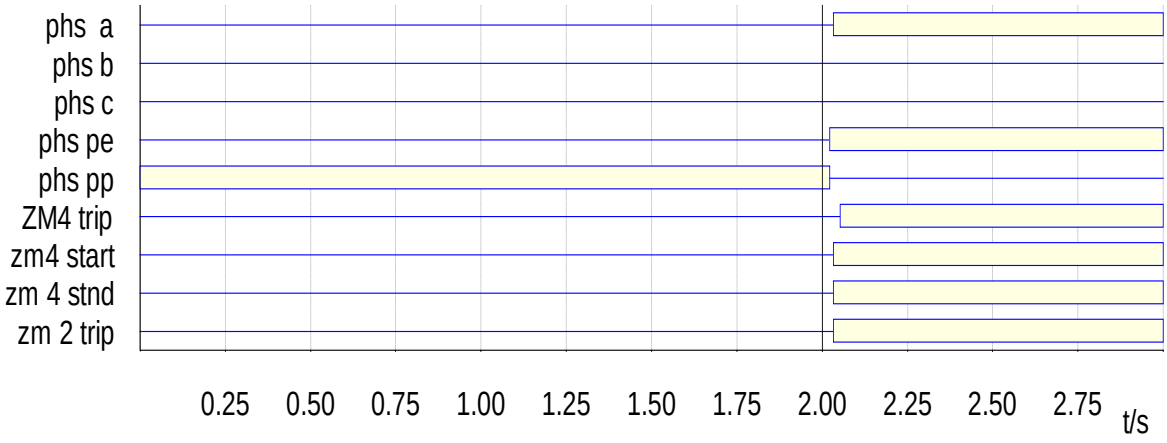

Figure 6.31: Binary operating signals for phase-to-earth fault in Figure 6.30

A fault was simulated at 50% of the first section of the Bacchus-Droërivier line. Relay operation was only obtained for a maximum resistance of 15 Ω primary (see Figure 6.30 and Figure 6.31). This fault resistance coverage is significantly smaller than what was obtained during load export conditions. There is therefore a definite differentiation between the resistive reach capabilities of the relay during load export and import conditions.

6.1.3.2.2 Phase-to-phase measurement

For a 30 Ω resistive fault at 50% of the first line section during the importing of both active and reactive power, the resistive reach limit of the relay was reached. (see Figure 6.32.) For a 35 Ω resistive fault at the same position only the phase selector measuring element detected the fault. (see Figure 6.34 and Figure 6.35).

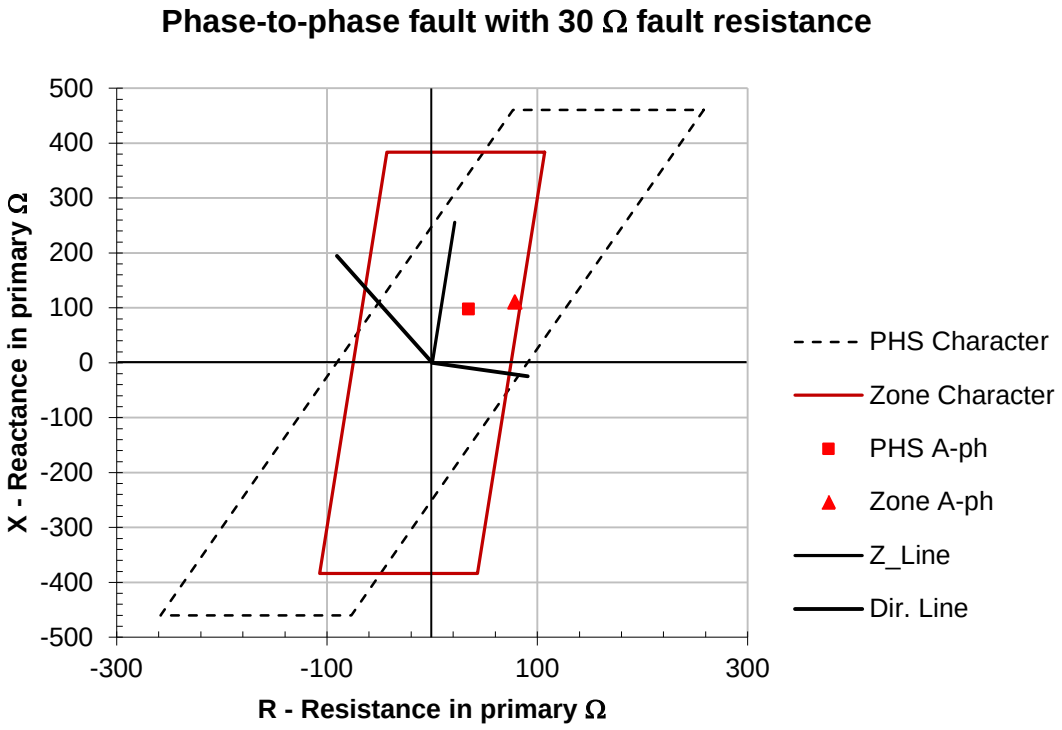

Figure 6.32: Phase-to-phase faults at 50% of first line section with importing MW and Mvar (a 30 Ω fault is shown)

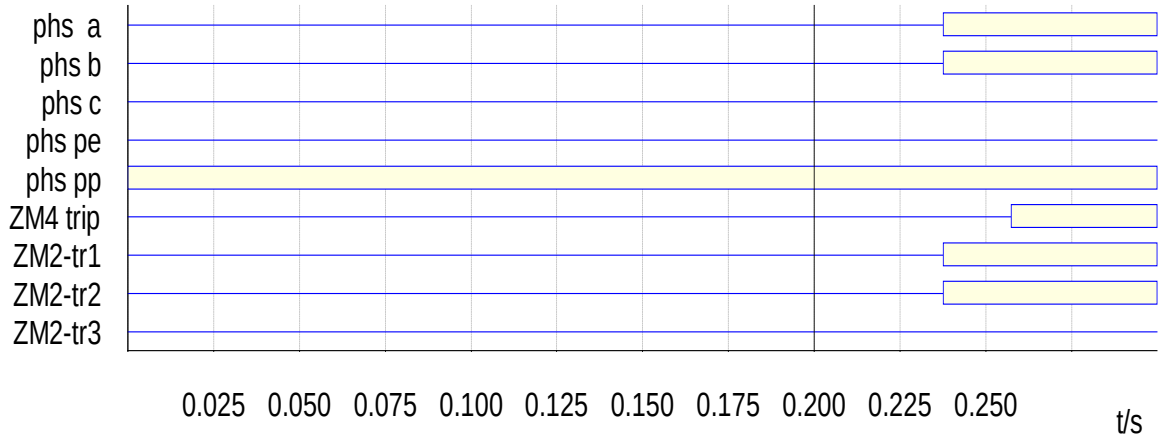

Figure 6.33: Binary signals for fault at 50% of first section of line

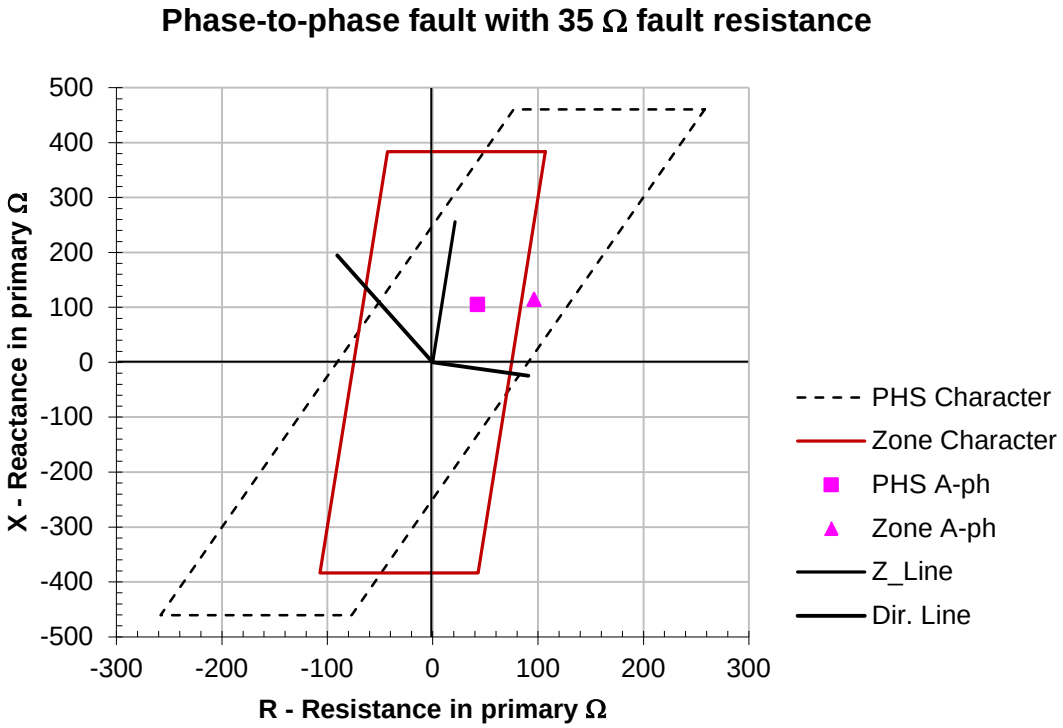

Figure 6.34: Phase-to-phase faults at 50% of first line section with importing MW and Mvar (a 35 Ω fault is shown)

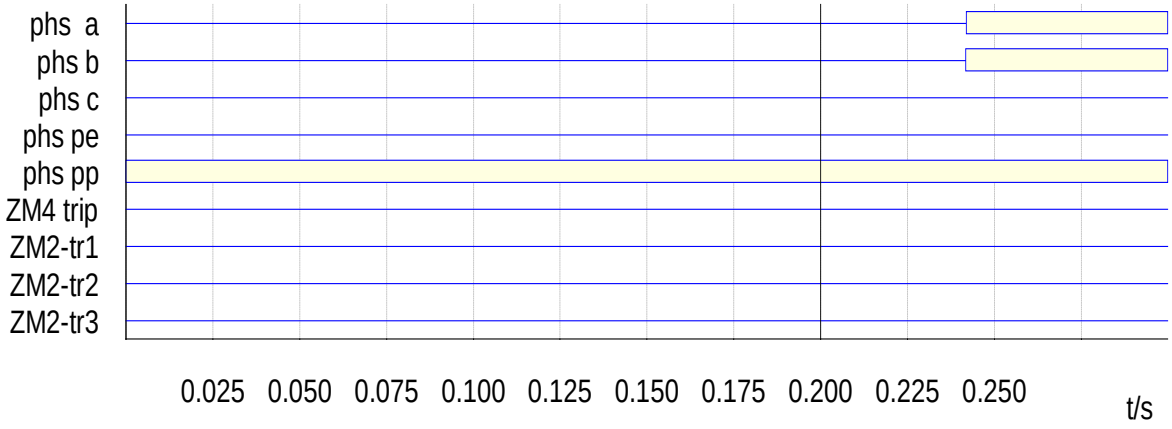

Figure 6.35: Binary signals for fault at 50% of first section of line

6.1.4 Conclusions

The results obtained for the zone-and phase selector reaches using the classic test method indicate that the relay operates correctly as per the applied setting. Slight underreaching is evident for the resistive reach towards the end of the reactive reach (see Figure 6.1 and Figure 6.2). The resistive reach of the phase-to-earth zone element is however not fully covered by the phase selector reach as per the latest available setting (see Figure 6.1). From the results shown in Table 6.1 for phase-to-earth faults with the remote end breaker in the open position, it is evident that the phase selector significantly underreaches in the resistive direction, whilst a significant difference in reach for the zone element is also illustrated. For the load export condition a higher resistive coverage for the zone element was obtained. Phase selector operation for a 5 Ω resistive fault at the end of the line was however still not obtained. Although this condition exists under high load export conditions, it is reason for concern since it indicates a lack of fault coverage on long lines and could result in long fault clearance times.

Fault resistance coverage for faults at 50% of the first line section were much reduced during load import conditions in comparison with that obtained during load export. Resistance coverage for faults at the end of the line could not be obtained during load import conditions. In fact no operation for line-end faults could be obtained during the load import conditions evaluated. The impact of remote end in-feed resulting in relay underreach must therefore not be underestimated and should

be further investigated. A definite difference exists therefore in the resistive reach coverage for phase-to-earth faults between importing and exporting conditions.

The results for a phase-to-phase fault shown in Table 6.2 at 100% of line length with the remote breaker in the open position show a serious underreach for the phase selector. A clear distinction can also be made for the resistive reach limits between load export and load import conditions. Considering the fact that remote end in-feed into a fault resistance will result in an increase in voltage at the fault position, which in turn will result in an increase in the overall fault impedance measured, it can be concluded that this would cause underreaching of an impedance measurement relaying device as is stated in literature. Since in the case of load import, the relay underreached significantly more than for the export condition, it can also be concluded that the influence of the direction and magnitude of load current must be considered.

Table 6.1: Phase-to-earth reach limits

Fault at % of line	R-reach breaker open	Element operation zone/ phs		R-reach MW & Mvar export	Element operation zone/ phs		R-reach MW & Mvar import	Element operation zone/ phs	
50% **	25	Y	Y	47.5	Y	Y	15	Y	Y
50% **	40	Y	N	50	N	N	17.5	N	Y
50% **	45	N	N						
100%	0	Y	N	5	Y	N			
100%	35	Y	N						
100%	40	N	N						

** - First line section.

Table 6.2: Phase-to-Phase Reach Limits

Fault at % of line	R-reach breaker open	Element operation zone/ phs		R-reach MW & Mvar export	Element operation zone/ phs		R-reach MW & Mvar import	Element operation zone/ phs	
50	55	Y	Y	65	Y	Y	30	Y	Y
50	60	N	Y	70	N	Y	35	N	Y
100%	0	Y	N						

6.2 SIEMENS 7SA513 Relay (Relay A)

In order to do a comparison between the actual relay reaches obtained through steady state secondary injection test methods, the impedance zone settings for this relay was reverse calculated from the overall loop impedance for the phase-to-earth loop obtained from the settings used for the REL531 relay for the overreaching zone. The relevant relay compensation factors $K_r = 4.54$ and $K_x = 1.81$ were calculated from the line impedance values provided in Chapter 6. Table 6.3 provides a comparative summary of the calculated settings. For the purpose of these tests the relay's load compensation setting was activated. Any impact due to load, as discussed in detail in section 3.2.7 should therefore be nullified by the relay.

Table 6.3: Reverse engineered settings comparison

7SA513 relay		**REL531 relay**	
Setting	**Secondary Ω setting**	**Setting**	**Secondary Ω setting**
R1BE	11.62 Ω	R1PE	7.04 Ω
X1B	84.17 Ω	X1PE	84.39 Ω
Re/Rl	3.54	R0PE	81.81 Ω
Xe/Xl	0.81	X0PE	288.24 Ω
		RFPE	20.8 Ω
R1B_Loop	52.763 Ω	R1PE_Loop	52.763 Ω
X1B_Loop	152.34 Ω	X1PE_Loop	152.34 Ω

Figure 6.36 presents the comparative relay reaches obtained with the relay settings as indicated in Table 6.3. The zone reaches for the two relays show identical reactive reach for the overreaching zone, whilst a slight reduction is observed in the resistive reach of the 7SA513 relay at maximum reactive reach with repect to the

theoretical curve shown for the REL531 relay. The resistive reach of the 7SA513 relay for close-up faults by far exceeds that of the REL531 relay.

The settings, as indicated for the 7SA513 relay in Table 6.3, were implemented on the relay and secondary injection tests performed to determine the impact of similar system conditions, that were used on the REL531 relay. The results of these tests are discussed in detail in the sections that follow.

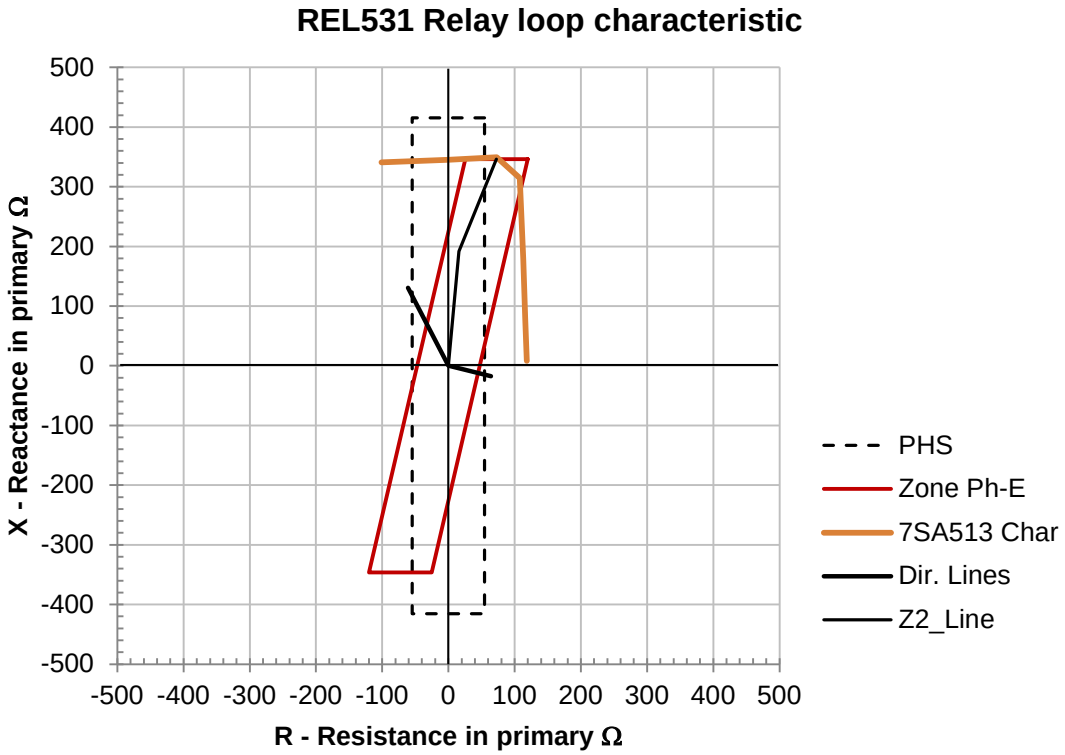

Figure 6.36: Tested relays phase-to-earth characteristic comparisson

6.2.1 Laboratory test results – classic method

6.2.1.1 Single-phase-to-earth – measuring elements

A radial system was used with no load connected with the result that for any fault on the feeder, the healthy phase currents are zero (i.e. the impact of charging and/or load current is ignored.) Similar to the REL531 relay, all impedances are shown in primary ohm per loop. Figure 6.37 presents the relay characteristics for the overreaching zone phase-to-earth measuring element as well as the fault detector reaches. Actual relay reach (test values) at different positions along the theoretical

phase-to-earth element reach is also indicated. Appendix I provides a comprehensive list of test results for different fault conditions and theoretical calculations.

The relay's resistive reach deviates increasingly from the theoretical characteristic for larger reactive reach values. A similar reduction in resistive reach was obtained for the REL531 relay. This is a normal occurance in relay measurements, is well documented and is not of concern.

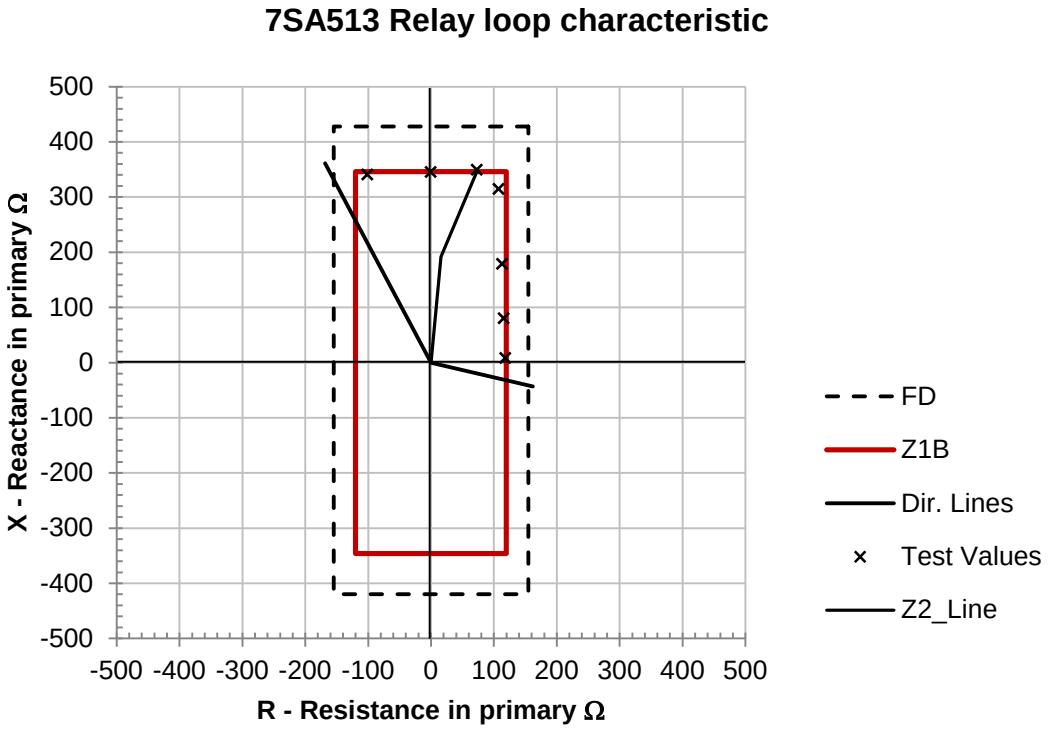

Figure 6.37: Phase-to-earth and fault detector characteristics with tested reach values

6.2.2 Impact of healthy phase currents on measurements

Utilising the same testing philosophy as was used during testing of the REL531 relay, the impact that the healthy phase currents would have on the actual performance of the relay during different system conditions was evaluated. The impact of healthy phase currents on the faulted phase was evaluated for the conditions of remote breaker open (capacitive charging), export and importing load currents.

6.2.2.1 Radial feed with remote breaker open (capacitive charging)

These tests were performed with the line series capacitor in and out of service. The Classic Shot Test indicated in Figure 6.38 performed with the series capacitor out-of-service, provides a reduced resistive coverage with increased reactance than those obtained with the standard text book test (no current on the healthy phases). The capacitive charging current on the healthy phases with the series capacitor by-passed therefore has an impact on the relay's resistive reach.

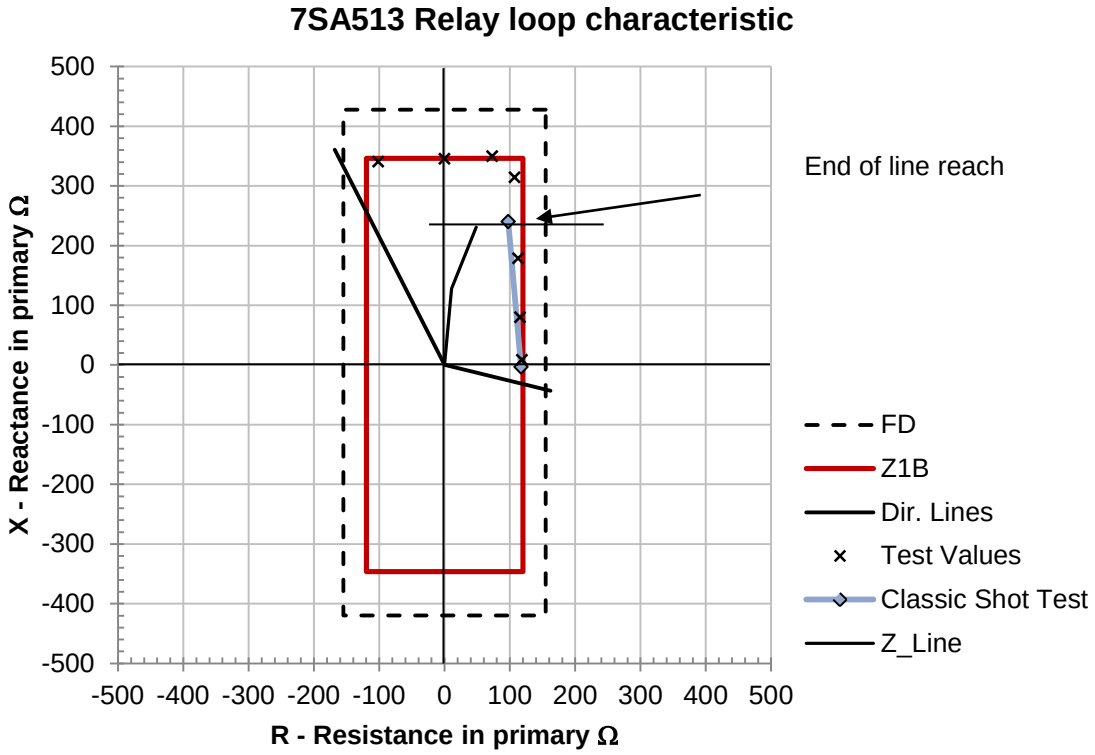

Figure 6.38: Classic shot test comparisson with remote breaker open

Some relay underreach (relay measures larger impedance values than actual to point of fault) in the reactive direction for a resistive end of line fault is observed with the series capacitor out-of-service.

Repeating the same reach tests, but with the series capacitor in service, provided a similar impedance reach for the close-up fault, but a different result for the end of line fault. The outcome of this test is graphically represented in Figure 6.39 whilst the results for both tests are statistically presented in Table 6.4 and Table 6.5. Fault and

post-fault conditions are shown in Table 6.4 and Table 6.5 as state 2 and state 3 respectively. Relay pickup was achieved for single-phase-to-earth resistive faults of 122 Ω and 121 Ω respectively with and without the series capacitor, at 10% of the first line section.

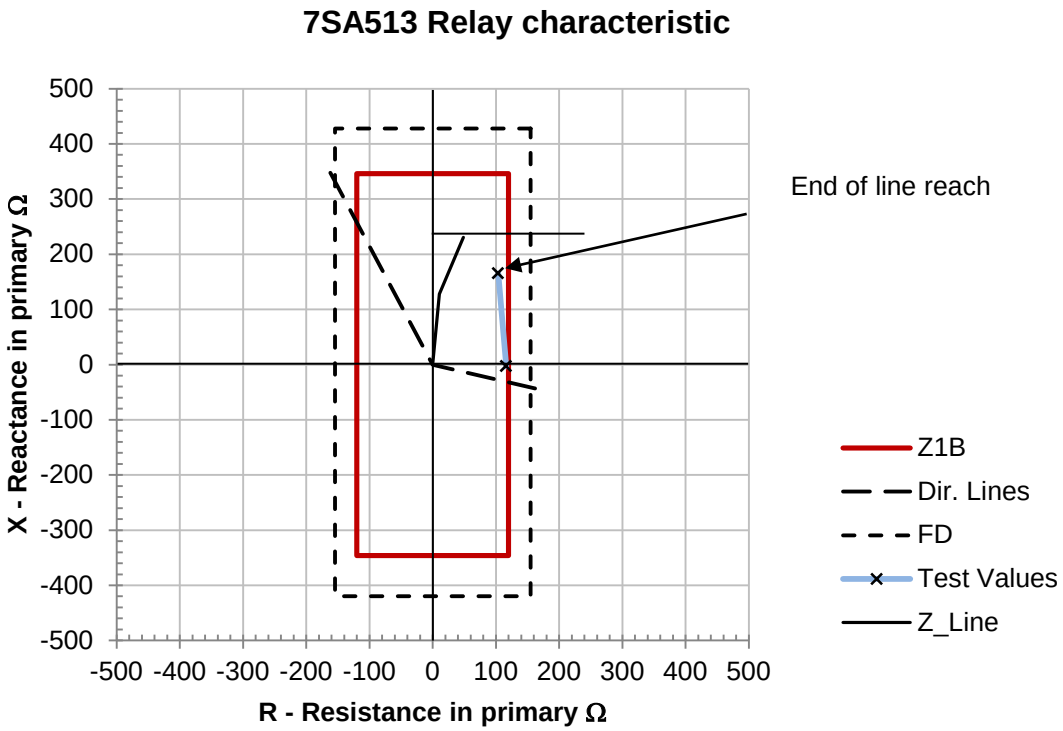

Figure 6.39: Classic shot test with series capacitor in service

Table 6.4: Capacitive charging test results - no series capacitor

State	State 1	State 2 (10%)	State 2 (100%)	State 3
V L1-E	230.9 kV 0.00° 50.000 Hz	218.52 kV -12.67° 50.000 Hz	206.59 kV -1.71° 50.000 Hz	230.9 kV 0.00° 50.000 Hz
V L2-E	230.9 kV -120.00° 50.000 Hz	234.47 kV -120.19° 50.000 Hz	232.37 kV -120.9° 50.000 Hz	230.9 kV -120.00° 50.000 Hz
V L3-E	230.9 kV 120.00° 50.000 Hz	229.87 kV 120.86° 50.000 Hz	233.43 kV 120.74° 50.000 Hz	230.9 kV 120.00° 50.000 Hz
I L1	352.47 A 89.69° 50.000 Hz	1.823 kA -2.26° 50.000 Hz	602.66 A -55.56° 50.000 Hz	320.0 A 89.73° 50.000 Hz
I L2	352.47 A -30.31° 50.000 Hz	358.85 A -30.79° 50.000 Hz	393.48 A -40.32° 50.000 Hz	320.0 A -30.27° 50.000 Hz
I L3	352.47 A -150.31° 50.000 Hz	351.98 A -149.16° 50.000 Hz	399.48 A -141.01° 50.000 Hz	320.0 A -150.27° 50.000 Hz
$Z_{(State\ 2)}$ R_F		117.17 - j3.262 Ω 122 Ω	97.58 + j240.47 Ω 61 Ω	

Table 6.5: Capacitive charging test results - series capacitor in service

State	State 1	State 2 (10%)	State 2 (100%)	State 3
V L1-E	230.9 kV 0.00° 50.000 Hz	218.42 kV -12.76° 50.000 Hz	202.81 kV -3.38° 50.000 Hz	230.9 kV 0.00° 50.000 Hz
V L2-E	230.9 kV -120.00° 50.000 Hz	234.48 kV -120.19° 50.000 Hz	233.33 kV -121.01° 50.000 Hz	230.9 kV -120.00° 50.000 Hz
V L3-E	230.9 kV 120.00° 50.000 Hz	229.87 kV 120.86° 50.000 Hz	233.37 kV 121.01° 50.000 Hz	230.9 kV 120.00° 50.000 Hz
I L1	342.11 A 89.71° 50.000 Hz	1.835 kA -2.72° 50.000 Hz	844.76 A -47.71° 50.000 Hz	342.11 A 89.71° 50.000 Hz
I L2	342.11 A -30.29° 50.000 Hz	348.23 A -30.76° 50.000 Hz	404.4 A -40.94.00° 50.000 Hz	342.11 A -30.29° 50.000 Hz
I L3	342.11 A -150.29° 50.000 Hz	341.61 A -149.16° 50.000 Hz	388.69 A -137.61° 50.000 Hz	342.11 A -150.29° 50.000 Hz
Z (State 2) R_F		116.36 – j3.16 Ω 121 Ω	103.47 + j165.13 Ω 61 Ω	

The reduction in the reactive reach pickup for the fault at the end of the line is a direct result of the capacitive reactance of the series capacitor, whilst the reduction in the resistive reach can only be attributed to the capacitive charging current of the line. Note that under normal conditions with no load connected, the healthy phase

charging currents are detected by the relay as load currents flowing towards the relaying point. This phenomenon will be discussed in more detail in the following sections.

6.2.3 Load current and remote in-feed

The following sub-sections discuss the export and import load scenarios used and the consequent response obtained from the relay.

6.2.3.1 Exporting MW and Mvar – remote breaker closed

6.2.3.1.1 Phase-to-earth measurement

The relay was exposed to the same test philosophy that was used for the REL531 relay, discussed in section 6.1.3.1. Test results obtained from the relay during load export conditions for resistive single-phase-to-earth faults with the series capacitor in by-pass mode are portrayed in Table 6. 6. The results shown are for faults at 10% and 100% of line length with the series capacitor by-passed. Note that the pre-fault load current (IL1) lags the voltage (V L1-E) by 29.66°, whilst during the single-phase-to-earth fault that follows in stage 2 this angle is reduced to the difference between -15.16° and -7.31°, which is directly attributed to the ratio of resistance in the fault and the reactance of the line to the point of fault.

The overall impact on the fault impedances measured for these faults with the series capacitor in by-pass mode is graphically illustrated in Figure 6.40. Relay measurements for close-up and line-end resistive faults of 119.54 Ω and 110.73 Ω with corresponding reactive reaches of 4.46 Ω and 240.37 Ω respectively were obtained. Proper distinction between these faults cannot be made based only on the calculated relay reaches, but when the actual fault resistances for which relay operation was obtained are considered, a different picture emerges. For the capacitive charging condition relay operation was obtained for resistive faults of 122 Ω at 10% of first line section length and 61 Ω at 100% of line length, whilst for the load export condition relay operation was obtained for a 132 Ω fault at 10% of first line section length and a 73 Ω fault at 100% of line length. The relay therefore is

able to detect faults of greater magnitude during load export conditions than during capacitive charging.

Results for the same faults with the series capacitor in service are shown in Table 6. 7 with a graphical representation in Figure 6.41. Note that the load current being transferred is now approximately twice that of the load with the series capacitor in by-pass mode. The resistive and reactive reaches measured for close-up and line-end faults are given by 118.77 Ω and 114.82 Ω for resistive and 9.12 Ω and 122.65 Ω for the reactive reaches respectively. Actual fault resistances of 146 Ω and 74 Ω were detected for the close-up and line-end faults. Overreaching phenomena are therefore highlighted for close-up resistive faults during load export condition with the series capacitor in service.

Table 6. 6: Test results during load export – series capacitor by-passed

State	State 1	State 2 (10%)	State 2 (100%)	State 3
V L1-E	242.5 kV 0.00 ° 50.000 Hz	236.5 kV -7.31 ° 50.000 Hz	232.8 kV 0.40 ° 50.000 Hz	242.5 kV 0.00 ° 50.000 Hz
V L2-E	242.5 kV -120.00 ° 50.000 Hz	242.9 kV -119.87 ° 50.000 Hz	244.5 kV -120.34 ° 50.000 Hz	242.5 kV -120.00 ° 50.000 Hz
V L3-E	242.5 kV 120.00 ° 50.000 Hz	241.8 kV 120.03 ° 50.000 Hz	242.8 kV 120.58 ° 50.000 Hz	242.5 kV 120.00 ° 50.000 Hz
I L1	751.4 A -29.66 ° 50.000 Hz	2.484 kA -15.16 ° 50.000 Hz	1.113 kA -56.39 ° 50.000 Hz	751.4 A -29.66 ° 50.000 Hz
I L2	751.4 A -149.66 ° 50.000 Hz	711.4 A -149.46 ° 50.000 Hz	765.4 A -139.19 ° 50.000 Hz	751.4 A -149.66 ° 50.000 Hz
I L3	751.4 A 90.34 ° 50.000 Hz	770.1 A 87.66 ° 50.000 Hz	633.9 A 84.14 ° 50.000 Hz	751.4 A 90.34 ° 50.000 Hz
Z (State 2) R_F		119.55 + j4.49 Ω 132 Ω	110.46 + j240.50 Ω 73 Ω	

Table 6. 7: Tests during load export - series capacitor in service

State	State 1	State 2 (10%)	State 2 (50%)	State 2 (100%)	State 3
V L1-E	230.9 kV 0.00 ° 50.000 Hz	225.4 kV -6.39 ° 50.000 Hz	218.8 kV -0.28 ° 50.000 Hz	219.0 kV -0.34 ° 50.000 Hz	230.9 kV 0.00 ° 50.000 Hz
V L2-E	230.9 kV -120.00 ° 50.000 Hz	231.6 kV -119.77 ° 50.000 Hz	234.0 kV -120.14 ° 50.000 Hz	233.4 kV -120.28 ° 50.000 Hz	230.9 kV -120.00 ° 50.000 Hz
V L3-E	230.9 kV 120.00 ° 50.000 Hz	229.8 kV 120.02 ° 50.000 Hz	229.9 kV 120.73 ° 50.000 Hz	230.7 kV 120.67 ° 50.000 Hz	230.9 kV 120.00 ° 50.000 Hz
I L1	1.560 kA -32.43 ° 50.000 Hz	2.981 kA -21.39 ° 50.000 Hz	2.095 kA -46.36 ° 50.000 Hz	2.096 kA -45.91 ° 50.000 Hz	1.560 kA -32.43 ° 50.000 Hz
I L2	1.560 kA -152.43 ° 50.000 Hz	1.497 kA -152.60 ° 50.000 Hz	1.487 kA -146.41 ° 50.000 Hz	1.533 kA -146.82 ° 50.000 Hz	1.560 kA -152.43 ° 50.000 Hz
I L3	1.560 kA 87.57 ° 50.000 Hz	1.597 kA 85.67 ° 50.000 Hz	1.474 kA 81.78 ° 50.000 Hz	1.452 kA 83.44 ° 50.000 Hz	1.560 kA 87.57 ° 50.000 Hz
Z (State 2) RF		118.78 + j9.12 Ω 146 Ω	114.72 + j117.64 Ω 132 Ω	114.82 + j122.65 Ω 74 Ω	

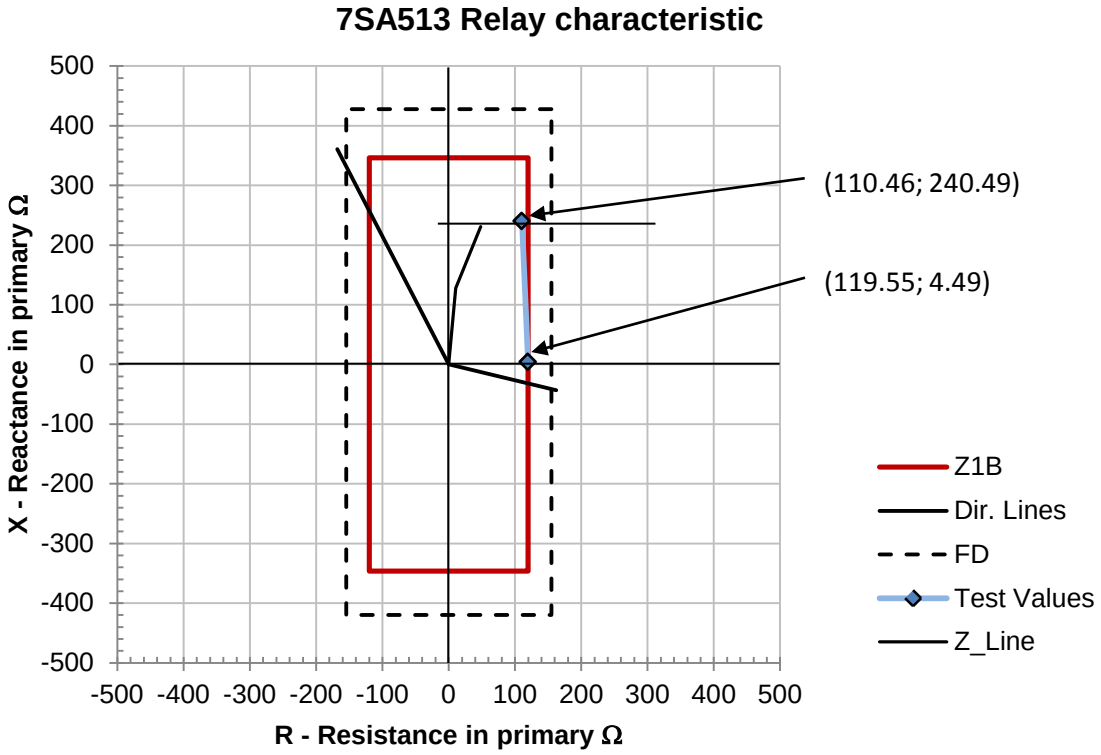

Figure 6.40: Relay reach during load export with series capacitor by-passed

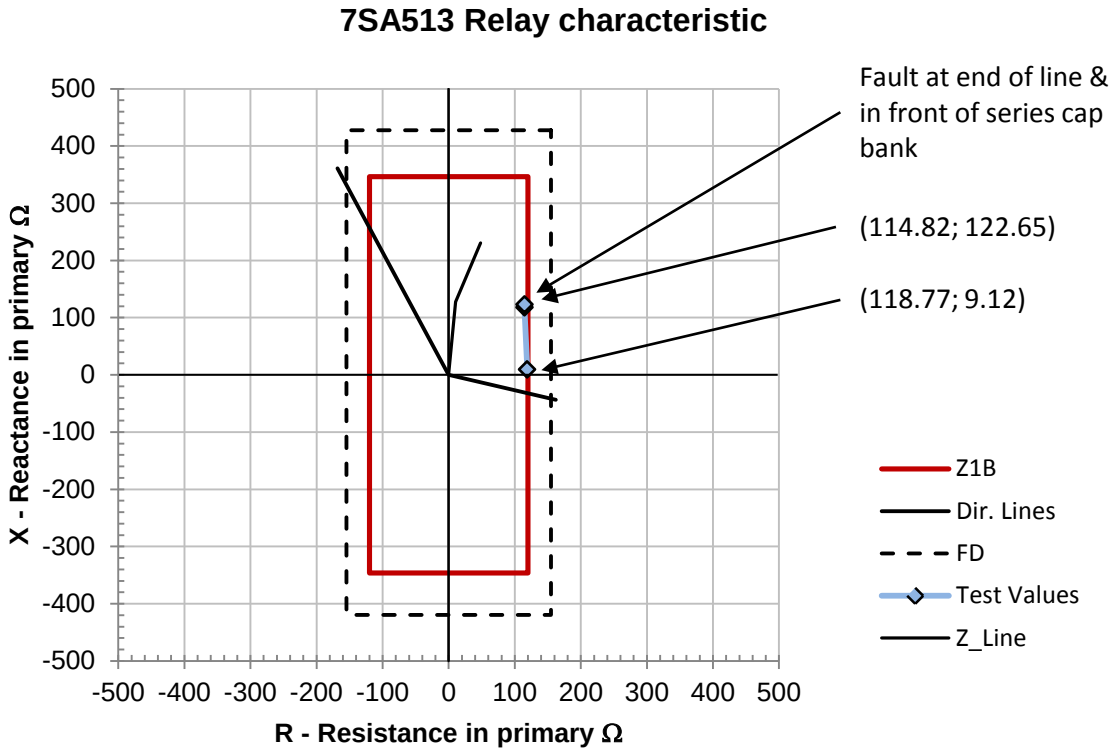

Figure 6.41: Relay reach during load export with series capacitor in service

The impact that exporting load current together with remote end in-feed has on the 7SA513 relay measurement has been discussed in detail in Chapter 3. The results of tests done on this relay during load export conditions is shown in Figure 6.42. Impedances measured for resistive faults of 136 Ω , 59 Ω and 28 Ω are indicated by the overall loop impedance values of 119.31 + j9.81 Ω, 115.18 + j105.83 Ω and 113.41 + j156.64 Ω respectively. These faults have been simulated at 10% of the first line section between Bacchus and Komsberg, at Komsberg series capacitor and at 50% of the next line section between Komsberg and Droërivier. With the series capacitor positioned on the line at a loop impedance reference value of 24.77 + j118.08 Ω, a definite overreach of the relay in the reactive reach was observed (105.83 Ω). For the resistive reach the relay underreaches since the actual line resistance and fault resistance at this point only adds up to a total loop resistive value of 83.77 Ω (24.77 Ω + 59 Ω), whilst the measured fault resistance equals 115.18 Ω.

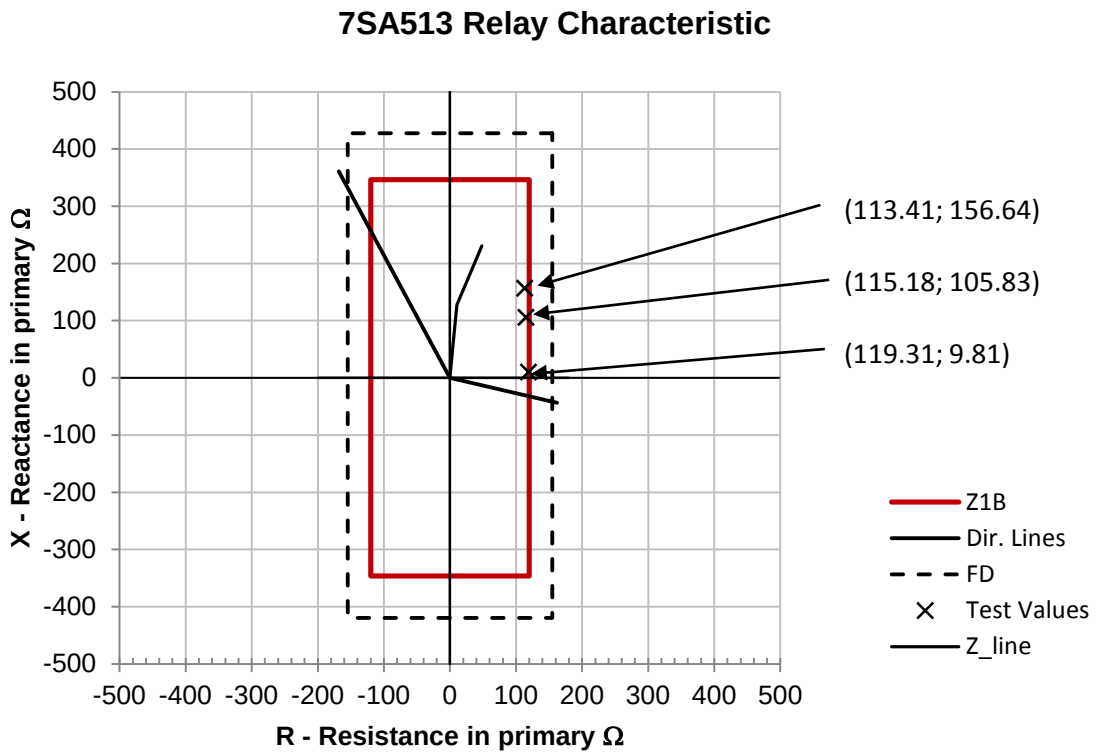

Figure 6.42: Relay reach during load export and dual in-feed conditions

Whilst the same can be said for the furthest fault away from the relay measuring position, the opposite is true for the closeup fault at 10% of the first line section. For this resistive fault of 136 Ω the relay measured an impedance of 119.31 + j9.81 Ω. The calculated loop line impedance together with fault resistance provides an impedance of 138.48 + j11.81 Ω. The relay measured smaller values in both resistance and reactance for this fault indicating an overreach condition in both cases. Table 6.8 provides a comprehensive summary of results obtained from tests at different locations along the line under specified system conditions. Resistance values indicated in this table refer to the maximum resistance for which relay operation was achieved at the specific point of fault. The next section will evaluate this relay's operation under load import with dual infeed system conditions.

6.2.3.2 Importing MW and Mvar – local breaker closed

6.2.3.2.1 Phase-to-earth measurement

The impact of imported load during dual in-feed system conditions were considered. Relay operation at different intervals along the line was evaluated. Fault resistance

was decreased until relay operation was obtained for each of the fault locations. Results of these tests are graphically represented in Figure 6.43 and illustrated in Table 6.8. Relay pickup for this system condition was only achieved for closeup faults at 10% of first line section, 50% of first line section and at Komsberg series capacitor bank.

The maximum fault resistance for which pickup was obtained at these fault positions were 102 Ω, 71 Ω and 45 Ω respectively. Relay operation was obtained at 117.86 + j18.24 Ω, 113.78 + j88.61 Ω and 108.86 + j160.9 Ω respectively. With the actual/calculated line impedance values of 104.48 + j11.81 Ω, 83.39 + j59.04 Ω and 69.77 + j118.08 Ω at the respective fault positions, relay operation occurred at values which exceed both the resistive and reactive values resulting in a clearly defined relay underreach condition.

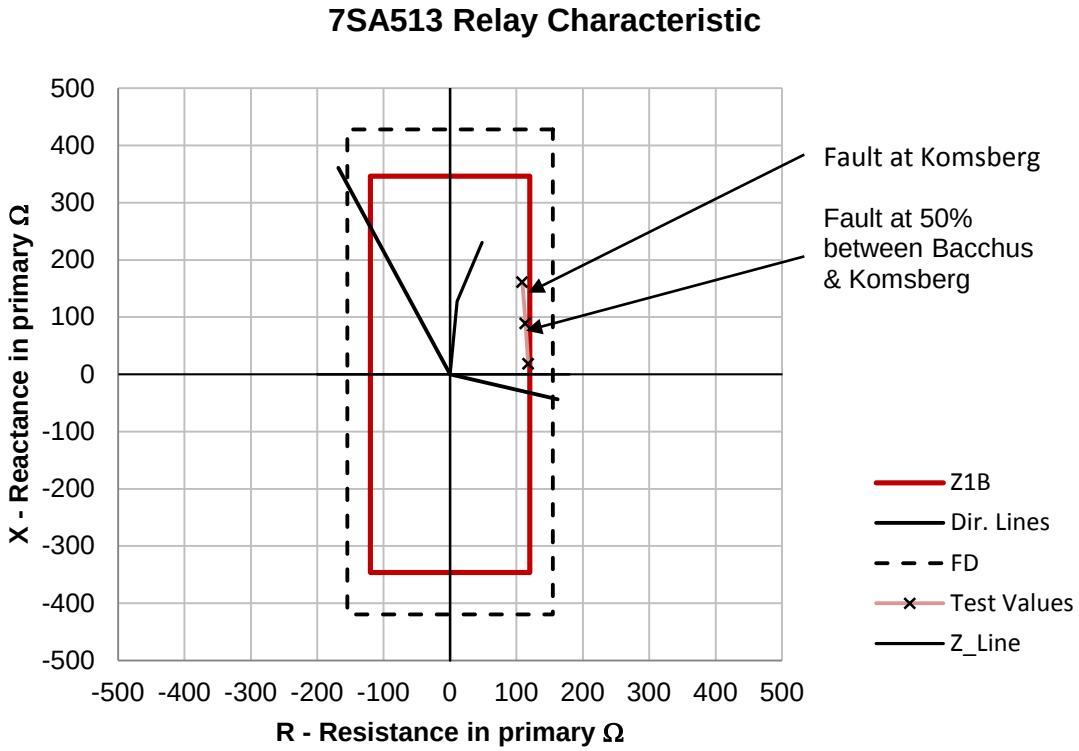

Figure 6.43: Relay operation during load import and dual in-feed system conditions

Table 6.8: Summary of fault resistances with measured and actual/calculated impedances per system condition

Fault Resistance(RF)	Position of Fault	Export Load, Radial Feed - Series Cap Bank By-Passed		Export Load, Dual Feed - Series Cap Bank By-Passed		Import Load, Dual Feed - Series Cap Bank By-Passed		Reach Result
		Actual	Measured	Actual	Measured	Actual	Measured	
132 Ω	10% *	134.477 + j11.808 Ω	119.550 + j4.49 Ω	-	-	-	-	O/R O/R
73 Ω	100%	121.423 + j230.813 Ω	110.464 + j240.499 Ω	-	-	-	-	O/R U/R
136 Ω	10% *	-	-	138.477 + j11.808 Ω	119.32 + j9.807 Ω	-	-	O/R O/R
59 Ω	Komsberg	-	-	83.772 + j118.079 Ω	115.29 + 105.833 Ω	-	-	U/R O/R
28 Ω	50% ***	-	-	64.598 + j174.446 Ω	113.43 + j156.64 Ω	-	-	U/R O/R
102 Ω	10% *	-	-	-	-	104.477 + j11.808 Ω	117.86 + j18.24 Ω	U/R U/R
71 Ω	50% **	-	-	-	-	83.386 + j59.039 Ω	113.78 + j88.61 Ω	U/R U/R
45 Ω	Komsberg	-	-	-	-	69.772 + j118.079 Ω	108.86 + j160.90 Ω	U/R U/R

*, ** - First line section, *** - Second line section

6.2.4 Conclusions

Although the relay's load compensation feature was enabled to allow automatic reactive reach correction thus ensuring more accurate fault impedance measurement, it was found that during load export conditions:

- the relay overreached in both resistive and reactive directions for closeup faults; and
- underreached for centre-of-line and end-of-line faults in the resistive direction whilst still overreaching in the reactive direction due to remote end in-feed.

During load import conditions it was found that the relay underreached for all faults in both the resistive and reactive directions. This is a clear indication that the relay's load compensation function does not fully cater for the load current under all system conditions. This is a phenomena that needs to be carefully evaluated when setting the relay in order to select the most appropriate relay settings, thus ensuring reliable operation. The relay user should evaluate whether the work done in this dissertation is sufficient for its own decision making, or initiate further research into this phenomena.